THESIS FOR THE DEGREE OF LICENTIATE ENGINEERING

Calibration Procedure and Industrial Applications of Coherence Scanning Interferometer

OLENA FLYS

Department of Materials and Manufacturing Technology
Chalmers University of Technology
Göteborg, Sweden 2016

Calibration Procedure and Industrial Applications of Coherence Scanning Interferometer
OLENA FLYS

Thesis for the degree of Licentiate of Engineering
ISSS 1652-8891
Report no. 107/2016

Published and distributed by:
Department of Materials and Manufacturing Technology
Chalmers University of Technology
SE - 412 96 Gothenburg, Sweden

Printed in Sweden
Chalmers Reproservice
Gothenburg, Sweden 2016

Telephone + 46 (0)31-772 1000

Calibration Procedure and Industrial Applications of
Coherence Scanning Interferometer
OLENA FLYS
Department of Materials and Manufacturing Technology
Chalmers University of Technology

Abstract

Countless industrial applications over the past decades have indicated the increased need to relate surface texture to surface function. Measurement and characterization of the areal nature of the surface allows the manufacturer to alter how the surface interacts with surroundings. Surface metrology covers the questions related to surface measurements, its analysis, representation, and interpretation. Despite the long experience of surface measurements there are still a lot of open questions. One of question was listed in this thesis is: "Is there a universal analysis technique available for understanding and interpreting the properties of surface topography?" The simple answer is: There is no universal analysis technique. However, for a better understanding and interpretation of the properties of a surface, a combination of different techniques can be necessary. The use of Power Spectral Density (PSD) analysis in this thesis showed to be a powerful analysis tool for identification of the differences and equalities between different instruments measuring similar topographies. This enables a selection of the proper instruments for measuring topographies with specific spatial frequencies or combination of frequencies.

Another focus area of this thesis was calibration of optical surface measuring instruments in particular Coherence Scanning Interferometer (CSI). The complexity of design of optical surface measuring instruments makes them difficult to calibrate. Since calibration procedure is an important part of quality control in the production, it is one of reason that those instruments are not used in production. The calibration procedure for the examining of some of the main metrological characteristics of Coherence Scanning Interferometry as an example of optical surface measuring instruments is discussed in this thesis. The concept of traceability is one of the fundamentals in metrology and assures the accuracy of measurements. The traceability and uncertainty are inseparable as it is impossible to compare measurements and hence calibrate instruments without statement of uncertainty. From the calibration procedure it was found that the dominant component for uncertainty estimation in the z-scale for CSI is the noise contribution and the dominant component for the x- and y- scale is the lateral resolution.
Future works based on the thesis results include to summarize good practice guide for users of CSI and a continued analytical and empirical study of the influence of spatial content of surfaces for different applications.

Keywords: Characterization, Coherence Scanning Interferometer, Power Spectral Density, uncertainty, 3D parameters.

Acknowledgements

I would like to express my thanks to all people who helped and supported me during my thesis work, especially:

First of all I would like to thank my supervisors, Bengt-Göran Rosén, Mathias Johanssson, and Lars Bååth without you this work would not have been possible.

I would like to express my gratitude to the funders of this project, Vinnova-Swedish Governmental Agency for Innovation Systems for financing my work. I am also grateful towards my employer SP Technical Research Institute of Sweden, who has given me opportunity to perform this work as an industrial Ph.D. student.

I would like to thank my department colleagues: Marianne Äremann, Agneta Jakobsson, Jan Elfström, Lena Gamalielsson, Gunn-Mari Löfdahl, Sten Bergstrand, Martin Zelan, Jan Johansson who create a nice and friendly environment and patiently supported my work.

I would like to thank my colleagues from Halmstad University: Sabina Rebeggiani, Zlate Dimkovski, Pär-Johan Lööf, for providing a creative and pleasant atmosphere.

Prof. Tom Thomas is the gentleman that took the time to give the valuable advice and make the language correct.

My beloved ones: Anders and Daniel for their patience, encouragement and understanding and to my family and friends inside/outside the academic world who have supported me and given me strength.

I also want to thank the following copyright holders for permission to use their material;

- SIS, Swedish Standards Institute for figure 6 and 22;
- IOP Publishing for figures 9,12,13,14;
- OSA Publishing for figure 17 and 18;
- Elsevier Ltd for figure 20.

List of appended papers

The results presented in this thesis are based on the work in the following appended papers:

Paper I: O. Flys, S. Källberg, G. Ged, Z. Silvestri, B.-G. Rosén, Characterization of surface topography of a newly developed metrological gloss scale, Surface Topography: Metrology and Properties, Volume 3, Number 4, September 2015.

Paper II: F. Glon, O. Flys, P.-J. Lööf, B.-G. Rosén, 3D SEM for surface topography quantification - a case study on dental surfaces, Journal of Physics: Conference Series, Volume 483, 14th International Conference on Metrology and Properties of Engineering Surfaces, 2013.

Paper III: O. Flys, Z. Dimkovski, B. Olsson, B-G. Rosén, L. Bååth, Piston ring topography variation and robust characterization, In: Proceedings of the 6th Swedish Production Symposium, Göteborg, Sweden, 2014.

Paper IV: O. Flys, L. Bååth, B.-G. Rosén, Calibration Procedure and Uncertainty Estimation for a Commercial White Light Interferometer, Accepted for publication in In: Proceedings of the 7th Swedish Production Symposium, Lund, Sweden, 2016.

List of symbols

ACF	Autocorrelation function
ACG	Areal cross grating
AFM	Atomic force microscopy
ASG	Areal surface grating
BIMP	International Bureau of Weights and Measures
CCD	Charge coupled device
CM	Confocal microscope
CMCs	Calibration and Measurement Capabilities
CMOS	Complementary metal oxide semiconductor
CSI	Coherence scanning interferometry
GPS	Geometrical product specifications
GUM	Guide to the Expression of Uncertainty in Measurement
IRP	Instrument response profile
ISO	International Organization of Standardization
ITF	Instrument transfer function
LED	Light emitting diode
LVDT	Linear variable differential transformer
NMI	National measurement institute
NPL	National Physical Laboratory
ODS	Optical dimensional standard
PDF	Probability density functions (PDF)
PSD	Power spectral density
PSDF	Power spectral density function
PSI	Phase shift interferometry
SEM	Scanning electron microscopy
SF	Structure function
SI	International System of Units
SPM	Scanning probe microscope
TEM	Transmission electron microscopy
WLI	White light interferometry
A	Autocorrelation function
Ax,y	Phase gap between two analysis results
ci	Sensitivity coefficient
E	Product of two measurements over the surface
$E1$	Statistical expectation of the squared height difference of two profiles
f	Focal length
fx	Components of the surface frequencies in x-direction
fy	Components of the surface frequencies in y-direction
g	Interference signal
h	Surface topography data
I	Interference
IAC	Modulation envelop function

Ii	Intensity of waves
Io(ζ)	Constant offset and co-sinusoidal function of signal
K	Interference fringes frequency
k	Angular wavenumber for the specific wavelength
kp	Expansion factor
l	Linearity error
n	Refractive index
NA	Numerical aperture
OPD	Optical path difference
P	Pupil radius
p	Interval of confidence
PSD	Power spectral density
q(K)	Non-zero positive part of the frequency spectrum
r	Lateral resolution of optical system
R	Object intensity reflectivity
Rref	Reference reflectivity
S	Structure function
S(ζ)	Envelop detection
S10z	Ten point height
S5p	Five point peak height
S5v	Five point pit height
Sa	Arithmetical mean height
Sal	Auto-correlation length
Sda	Closed dale area
Sdq	Root mean square gradient of the scale limited surface
Sdr	Developed interfacial area ratio of the scale limited surface
Sdv	Closed dale volume
Sha	Closed hill area
Shv	Closed hill volume
Sk	Kernel roughness depth (roughness depth of the core)
Sku	Kurtosis
Smc (mr)	Inverse areal material ratio of the scale-limited surface
Smq	Material ratio
Smr (mc)	Areal material ratio of the scale-limited surface
Smr1	Upper material ratio
Smr2	Lower material ratio
Sp	Maximum peak height
Spc	Arithmetic mean peak curvature
Spd	Density of peaks
Spk	Reduced peak height (roughness depth of the peaks)
Spq	Root mean square gradient of the scale limited surface
Sq	Root mean square height
Sqnoise	Root mean square height of noise
Sq flat	Root mean square height of measurement on flat

Ssk	Skewness
Std	Texture direction
Str	Texture-aspect ratio
Sv	Maximum pit height
Svk	Reduced valley depth (roughness depth of the valleys)
Svq	Dale root mean square deviation
Sz	Maximum height
t	t-Distribution
u	Standard uncertainty
U	Expanded uncertainty
U(β)	Distribution of light in pupil
uc	Combined (standard) uncertainty
V(k)	Detectional spectrum
Ve f f	Degrees of freedom
Vm(p)	Material volume
Vmc	Core material volume of the scale limited surface
Vmp	Peak material volume of the scale limited surface
Vv(p)	Void volume
Vvc	Core void volume of the scale limited surface
Vvv	Pit void volume of the scale limited surface
X	Distinct input quantities
Y	Single measurand
z	Height position for profile data
α	Amplification coefficient
β	Directional cosine of angle ψ
ζ	Specific point of image
θ	Half aperture angle
λ	Mean wavelength of the light source
ϖ	Offset of CSI optical system parts
$\rho(k)$	Frequency spectrum
τ	Distance between two profiles
ϕ	Phase difference between waves
ψ	Incident angle

Contents

Abstract I
Acknowledgements III
List of appended papers V
List of symbols VI
1 INTRODUCTION 1
1.1 BACKGROUND 1
1.2 AIM OF THE THESIS 1
1.3 RESEARCH QUESTIONS 1
1.4 APPROACH 2
1.5 DELIMITATIONS 2
1.6 GENERAL MEASUREMENTS CONDITIONS 2
1.7 THESIS STRUCTURE 3
2 UNCERTAINTY AND METHODS OF ITS DETERMINATION 5
2.1 INTRODUCTION 5
2.2 TRACEABILITY 6
2.3 EXPRESSION OF UNCERTAINTY IN MEASUREMENTS 7
2.4 DEFINITIONS RELATED TO UNCERTAINTY 8
2.5 METHODS OF CALCULATION UNCERTAINTY 10
3 SURFACE CHARACTERIZATION 13
3.1 INTRODUCTION 13
3.2 MEASUREMENT TECHNIQUES 14
3.2.1 CONTACT PROFILERS 14
3.2.2 NONCONTACT PROFILERS 16
3.3 CHARACTERIZATION METHODS 19
3.3.1 SURFACE ROUHNESS PARAMETERS 19
4 COHERENCE SCANNING INTERFEROMETRY (CSI) 25
4.1 INTRODUCTION 25
4.2 FORMATION OF WHITE LIGHT FRINGES 25
4.3 WORKING PRINCIPLES 26
4.4 INTERFERENCE OBJECTIVES 27
4.5 SIGNAL FORMATION FOR SURFACE RECONSTRUCTION 28
4.6 SIGNAL PROCESSING 30
4.7 SURFACE MEASUREMENTS PROBLEM 32
5 CALIBRATION PROCEDURE OF WHITE LIGHT INTERFEROMETER 33
5.1 INTRODUCTION 33
5.2 INSTRUMENT NOISE DETERMINATION 35
5.3 FLATNESS DEVIATION OF AREAL REFERENCE 36

5.4 AXIAL CALIBRATION 37
5.4.1 Z-AXIS CALIBRATION 37
5.4.2 X AND Y-AXIS CALIBRATION 38
5.5 RESOLUTION 39
5.5.1 DEFINITION OF LATERAL PERIOD LIMIT AND INSTRUMENT TRANSFER FUNCTION 39
5.5.2 DETERMINATION OF LATERAL PERIOD LIMIT 41
6 RESULTS AND DISCUSSION 43
6.1 POWER SPECTRAL DENSITY (PSD) (PAPER1 Characterization of surface topography of a newly developed metrological gloss scale) 44
6.2 SURFACE ROUGHNESS PARAMETERS (PAPER 2 - 3D SEM for surface quantification- a case study on dental implant) 46
6.3 SURFACE CHARACTERISATION AND UNCERTAINTY INFLUENCE ON RESULTS (PAPER 3 Piston ring topography variation and robust characterization) 47
6.4 CALIBRATION OF COMMERCIAL INSTRUMENT (PAPER 4 Calibration procedure and uncertainty estimation for a commercial white light interferometer) 48
7 CONCLUSIONS AND FUTURE WORK 51
7.1 CONCLUSIONS 51
7.2 FUTURE WORK 51
REFERENCES 53

1 INTRODUCTION

1.1 BACKGROUND

Over the years control of surface topography has been of vital importance for manufacturing, engineering and scientific disciplines. The characterization and evaluation of engineering surface texture has constituted a challenging metrological problem that has remained open so far. Surface metrology is the branch of science that is concerned with the measurement and characterization of surface topology. It covers the questions related to the measurement results, their representation and interpretation, the appropriateness of techniques used for measurements, measurements applications, relationship between result analysis and the function of surface [1]. Many efforts have been made in this area for instance new ISO standards have been published in the 3D (areal) measurement field, but still much remains to verify and further develop in the area [2].

In recent years the capability of surface measuring instrument has been greatly extended by further development of scanning probe techniques and optical instrumentation that is still considered as emerging technology. Surface measurements by using optical techniques are of great interest for industry and science. This area is growing rapidly thanks to innovations in the manufacturing of improved instruments, the extended capacity of processing software and the numerous publications on development of techniques [3]. However optical surface measurements techniques are still slowly accepted in production due to the lack of standardization and missing comparability to tactile methods. It has been clear for the scientists and experts in the field that proper calibration methodology for the given instruments is required [4]. So far no accepted standardized solutions exist for determination of measurement uncertainty. An important issue that must be addressed to bring surface topography into compliance with manufacturing quality systems, is the measurement traceability of the instruments.

1.2 AIM OF THE THESIS

The aim of the thesis is to increase the current knowledge of the interaction between surfaces and the optical metrology of surfaces topographical properties with the following sub goals:

- apply appropriate tools and methods for quantitative characterization of surfaces measured by Coherent Scanning Interferometers (CSI);
- develop and test a metrology framework for general calibration and adjustments of CSI;
- Propose rules for determination of uncertainty budgets for measurement using CSI.

1.3 RESEARCH QUESTIONS

The following three research questions have been guiding the thesis work and form a logical “red thread”, connecting the results from the four appended papers into the integral work.

1. Is there a universal analysis technique available for understanding and interpreting the properties of surface topography?
2. What main procedures are needed to be specified for the interferometric measurements of the chosen applications?
3. What uncertainty factors are influencing the interferometric measurements of surface topography in general?

1.4 APPROACH

The relationship between surface function manufacturing processes and surface characterization may be described as shown in Figure 1. For each loop, new knowledge is gained. All three facets of the control loop in Figure 1 must be connected in order to understand the relationship and produce well-functioning surfaces. This main focus of this thesis is the *Characterization* facet from Figure1. The process of characterization and evaluation of surface texture depends on a number of factors. This thesis covers the influence of the measurement instruments' metrological characteristics on measurement results; parameters and analysis techniques used for representation of measurement results; and the interpretation of measurement results for different applications. The optical technique represented by Coherence Scanning Interferometry (CSI), its calibration procedure for determination of the main metrological characteristics and the estimation of the uncertainty budget is included in the main part of the thesis. In addition, analysis and comparison of measurement results using surface parameters and Power Spectral Density (PSD) techniques, performed by CSI and other techniques, as well as application of CSI for production control of surface topography are areas covered in this thesis.

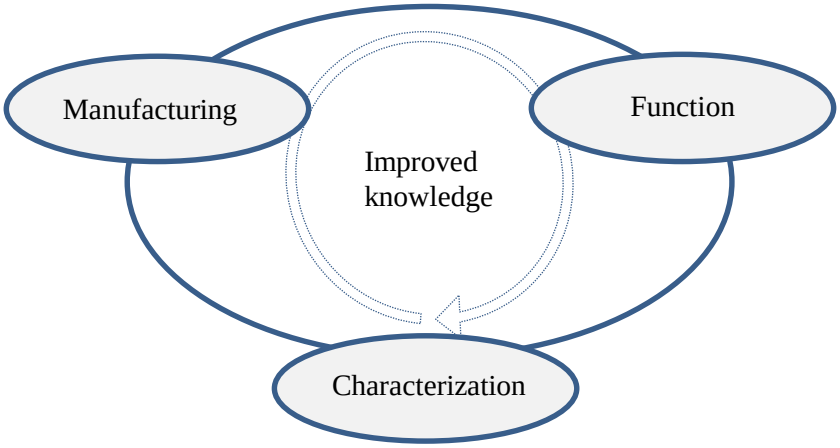

Figure1: *The relationship between the manufacturing, function and characterization adapted from [5].*

1.5 DELIMITATIONS

- Determination of uncertainty budgets has been done using the framework proposed by GUM ("The Guide to the expression of uncertainty in measurement"). The Monte Carlo method for measurement uncertainty evaluation has not been applied in this work.
- Line-profiling methods and areal integrating methods used for surface topography measurements are not covered by this thesis.

1.6 GENERAL MEASUREMENTS CONDITIONS

- Environmental conditions: the measurements have been performed in a laboratory with air temperature control. The temperature was 20±1°C, and measured humidity was 50±15%RH.
- Standard artifacts used in study excluding the ASG (Areal Surface Grating) standard have been calibrated and traceable to the realization of the metre at SP Technical Research Institute of Sweden (National Metrology Institute) in Borås.

1.7 THESIS STRUCTURE

Chapter 1 gives the introduction to the thesis including the background, objectives and limitations.
Chapter 2 presents the methods for expressing and estimating uncertainty in measurement, based on the definition and prescription given by GUM.
Chapter 3 gives an overview of some existing surface measurement and characterization techniques.
Chapter 4 describes the working principle and some limitations of CSI.
Chapter 5 presents the methodology for the calibration of CSI.
Chapter 6 is the summary of the results discussed in different aspects.
Chapter 7 includes the conclusions drawn from the studies and future work.

The graphical representation of thesis structure shown in Figure 2.

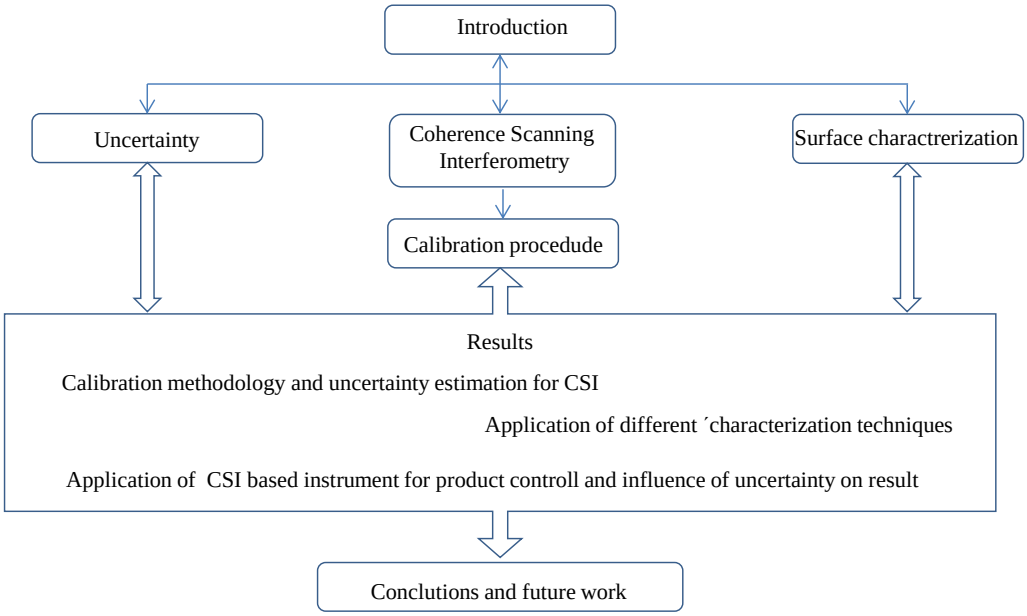

Figure 2: *Thesis structure*

2 UNCERTAINTY AND METHODS OF ITS DETERMINATION

2.1 INTRODUCTION

Measurements are an important aspect in decision making, communication of technical information, establishing scientific facts, monitoring manufacturing processes and maintaining human and environmental health and safety. Both industry and governments make big investments to acquire, install, maintain and develop test and measurement equipment. The more critical the applications are the higher are the requirements on measurement quality assurance. But how "correct" are the measurement results in these various applications upon which critical decisions are made?

Uncertainty encountered in the measurement process is the key aspect in measurement quality and defines the quality of the measurement result, i.e. a figure indicating how much confidence we can put in a result. Figure3 illustrate a typical measurement cycle and it's components in combination with result based decisions.

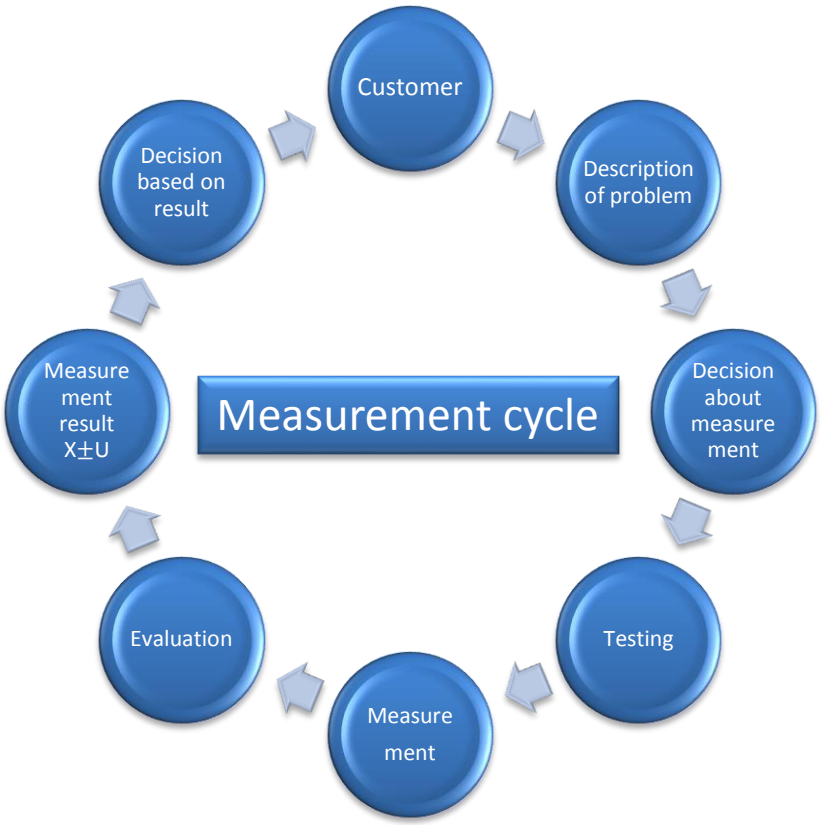

Figure 3: *Measurements cycle components and their influence on decision making.*

There will always be an uncertainty in the value of the result. Nothing but the definition of a quantity (i.e. the metre) is exact. Received or measured values always include systematic and random errors. Even when correction of a systematic error has been applied to the estimation of the result there will still be an uncertainty in this correction. Due to the fact that the measurement environment is not perfectly stable, there will always be an uncertainty arising from the random factors.

Why is uncertainty important?

The objective of estimation of uncertainty is to assess reliability of received measurement results, and to give us knowledge of the confidence that can be coupled to the decisions based on the measured result. The estimation of uncertainty allows meaningful comparisons of measurement results from different sources (reference value given by standard and result from laboratory). Accurate measurements and decisions made with low risk require the presence of standards (reference) of measured value and evaluation of uncertainties in the measurement process. This is essential in all areas of science and technology. By accurate measurements we mean the quality-assured measurements with properly identified and quantified uncertainty that will lead to new discovery and recognition for scientific society. For the engineering community it leads to improved safety margins in complex systems. To provide a quality-assured measurement it needs to include metrological traceability and measurement uncertainty.

2.2 TRACEABILITY

Industry requires that manufactured products perform reliably. This implies that the relevant physical properties of their components or product must be certified and verified against local standards which are a part of the traceability chain to international standards of measurement. International certification depends on the existence of standards of measurement in every field of science and technology. The country's national measurement institute (NMI) is responsible to provide maintenance, development and research into standards of measurement at the highest possible level of accuracy needed by the industry or society in the country. This means that the NMI transfers the traceability from the definition of the quantity to the industry and assuring the quality in this service by participation in international intercomparisons. The areas where a specific NMI has a mutual recognition with other NMIs is presented in a database where the Calibration and Measurement Capabilities (CMCs) are listed [6].

In turn the degree to which the participating NMIs' standards 'agree with one another' or, more formally, have the essential property of 'mutual equivalence' is determined by international comparisons and is a decision made by the BIPM (Bureau International des Poids et Measures, or International Bureau of Weights and Measures, in Paris) [7]. Figure 4 demonstrates the metrological traceability chain.

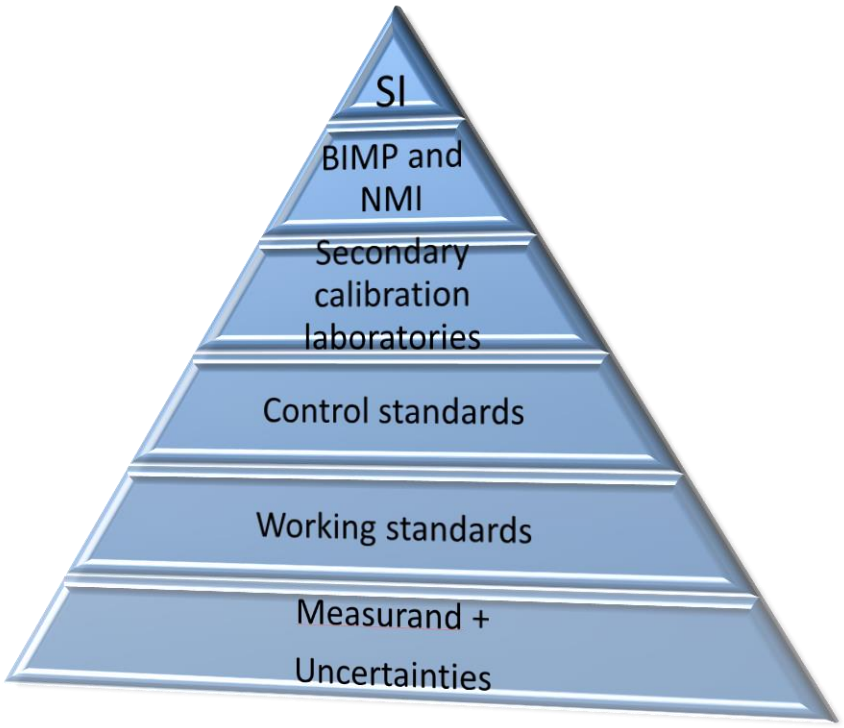

Figure 4: *Metrological traceability chain.*

Metrological traceability: "property of a measurement result whereby the result can be related to a reference through a documented unbroken chain of calibrations, each contributing to the measurement uncertainty" [8]. Metrological traceability includes six important elements that confirm it definition: an unbroken chain; uncertainty of measurement; documentation; reference to SI unit; calibration interval.
It is important that measurement systems validation procedure should include all six elements to establish metrological traceability. Companies need to ensure that measurements performed correctly via validation of their measurement systems. It should be done to evaluate their products, services or equipment (for safety, quality, protection of health and the environment).

2.3 EXPRESSION OF UNCERTAINTY IN MEASUREMENTS

Valid results, used as a base for decisions, trade, legal actions or publications, must not be a stroke of luck but should get their authenticity by a carefully determined figure of merit. The characteristic needed for all kinds of measurements is the measurement uncertainty. Its necessity was realized first in physics and later in chemistry, therefore an important document, "The Guide to the expression of uncertainty in measurement", (GUM or Guide) has been published in 1993 [8] (corrected and reprinted in 1995and 2008 and 2010), [9,10] with a number of detailed examples taken from physical measurement problems.[11] The main purpose of this document was to be applicable for broad spectrum of measurements for:
- Retention of quality and assurance control in production;
- Complying the law and regulation;
- Implementation of basic and applied research in science and engineering;
- Development, maintaining and calibration of reference standards (both national and international);
- Caring out activities to achieve traceability to national standards.

GUM supplies the users with general rules for evaluation and expression of uncertainty that explain its wide spread and acceptance. Another reason is that seven international

organizations that dealing with the fundamentals of metrology have been involved in development of GUM: [12]
BIMP (International Bureau of Weight and Measures, www.bimp.org);
IEC (International Electrochemical Commission, www.iec.ch);
IFCC (International Federation of Clinical Chemistry, www.ifcc.org);
ISO (International Organization of Standardization, www.iso.ch);
IUPAC (International Union of Pure and Applied Chemistry, www.iupac.org);
IUPAP (International Union of Pure and Applied Physics, www.iupap.org);
OIML (International Organization of Legal Metrology, www.oiml.org).

GUM include main guidelines and recommendation to identify factors that affect the measurement uncertainty and quantify them afterwards in a statistical sense by assigning proper probability density functions (PDF) with suitable parameter settings to quantitatively describe the uncertainty. The functional relationship of the influence quantities are expressed using mathematical equations, the so-called equation of the measurand. The uncertainty framework described by GUM is appropriate for application for a limited set of measurement scenarios, but actually they appear very often in practice. However it has been identified some drawback of the evaluation method, one is that information about probability distributions used to describe influence quantities is reduced in only using the first two moments – mean value and standard deviation – of the distributions for evaluation. Another shortcoming is that the measurement model has to be linear or must be linearized for evaluation, which means that the measurement model is kept as simple as possible. Another recommendation is to use only most important influences for measurement uncertainty evaluation. Therefore, the decision with regard to which influence quantities can be neglected and which are important is no trivial task. [13]

2.4 DEFINITIONS RELATED TO UNCERTAINTY

Measurement as described by GUM includes method of measurement and measurement procedure to determine the value of the quantity to be measured.
As a measurement never is exact it includes errors. Errors can be divided into two groups: systematic and random. *Random errors* in experimental measurements are caused by unknown and unpredictable changes in the experiment. The random errors cannot be compensated for, but their influences can be reduced by increasing the number of observations. *Systematic errors* are difficult to eliminate because they cannot be distinguished statistically and need to be found by other methods. When identified, systematic effects can, and should, be reduced by applying corrections. The GPS standards, such as [14], describe various types of errors which regularly show up in measurement results, including systematic and random error, drift and outliers.
The estimation of uncertainty is based on the assumptions of probability theory and follows "the results of measurements have been corrected for all recognized significant systematic effects". So GUM 's definition of uncertainty that is generally accepted today: "Uncertainty (of measurement) is a parameter, associated with the result of a measurement that characterizes the dispersion of the values that could reasonably be attributed to the measurand", can be related to random effects.
GUM suggests two different ways for evaluation of uncertainty: type A and type B.
The evaluation of uncertainty by the statistical analysis of series of observations is termed a *Type A evaluation (of uncertainty).* This method can be applied when significant number of measurements is obtained and the measurement procedure repeats under similar measurements conditions, and result can be characterized by experimental standard deviation.

Example of *Type A* uncertainty estimation for hardness measurements from the single measurement is described below:[15]
Measurements have been performed using previously calibrated Rockwell hardness operating system.
10 indentations were made on the test block with results listed in table1.

Table1: *Result of Rockwell hardness measurements.*

Measurement number	1	2	3	4	5	6	7	8	9	10
Hardness value (HRC)	45,4	45,5	45,4	45,3	45,5	45,3	45,3	45,4	45,4	45,4

Calculated statistical parameters are:
Mean value 45,39 HRC
Estimated standard deviation ±0,074 HRC
For described hardness experiment standard deviation contribution is multiplied with sensitivity coefficient 1,06 pre-defined for the 10 observation and k=1.
So standard uncertainty estimated by *Type A* method will be:

$$u(x) = 1{,}06 * \pm 0{,}074\ HRC = \pm 0{,}078 HRC$$

The evaluation of uncertainty from an assumed probability distribution where the component of uncertainty can be based on experience or on other information is termed a *Type B* evaluation *(of uncertainty).* This method is based on scientific judgments of information from different sources such as: previous measurement data; experience or general knowledge about material or instrument; manufacturer's specifications; data from calibrations or other reports; etc. For evaluation of standard uncertainty *Type B* it is most useful to use four types of distribution for transforming limits of variation into the standard deviation [14].
These types are:
Gauss distribution that can be described by equation: $u(x) = {}^{e}/_{2}$
Rectangular or uniform distribution: $u(x) = {}^{e}/_{\sqrt{3}}$
U-shaped distribution: $u(x) = {}^{e}/_{\sqrt{2}}$
Triangular distribution: $u(x) = {}^{e}/_{\sqrt{6}}$

Example of *Type B* establishment of standard uncertainty from calibration certificate:[15]
Accordingly to the calibration certificate for an instrument used in a test the measurement uncertainty over its range of calibration is ±0.1% at a 95% confidence level.
A coverage factor is k = 2 for the 95% confidence level. So the contribution of standard uncertainty from the instrument calibration throughout its calibrated range is:

$$u(x) = \pm\left(\frac{0{,}1}{2}\right) = \pm 0{,}05\%$$

of the reading.
Uncertainty estimation achieved by using method type A or B usually called standard uncertainty that need to be separated from combined standard uncertainty and expanded uncertainty.
Uncertainty of the result represented by (single) standard deviation is **standard uncertainty, "u"**
Uncertainty of result represented as combination of standard uncertainties is **combined (standard) uncertainty, "u_c"**
Uncertainty of result represented as combined (standard) uncertainty multiplied with coverage

factor k (typically: k = 2) providing a level of confidence of approximately 95 % is **expanded uncertainty, "U"**.

Example of calculation standard, combined and expanded uncertainty:

Example of *Type A* estimation of uncertainty will be completed with following information:

-The intender had been verified to 0.3 HRC and the depth measuring device to 0.1 HRC.

-The machine used for measurements have been verified against standardized machine. The standardizing machine has been verified to 0,5HRC.

- The uncertainty associated with the total force, which was better than +0.1%, gave a negligible contribution to the total uncertainty (<0.01 HRC), as did the uncertainty associated with the diameter of the indenter balls.

The functional relationship for the measurement was identified as a linear combination. A coverage factor of k = 2 for 95% probability has been used for calculation of expanded uncertainty. The table 2 demonstrate result of calculation [15].

Table 2: *Example of calculation expanded uncertainty for hardness measurement.*

Source of Uncertainty	Standard Deviation	Divisor (distribution type)	Sensitivity Coeff.	Standard Uncertainty
Type A Single reading of hardness	±0,074	1	1	±0,078
Type B Indenter verification	±0,03	√3	1	±0,017
Indenter measurement	±0,10	√3	1	±0,058
Standardising machine verification	±0,50	√3	1	±0,289
Combined uncertainty	±0,305			
Expanded uncertainty, k=2	±0,61			

2.5 METHODS OF CALCULATION UNCERTAINTY

The first step for calculation of measurement uncertainty for the given measurement scenario is to identify, collect and organize all information related to the measurement and measurement uncertainty. The first thing to do is to define the quantity that should be measured and is of interest. The next step requires a detailed analysis of the environment and specifies all the influence quantities that contribute to the uncertainty of the measurement. Usually, a measurement follows given measurement protocols and/or specifications, but those documents often describe only the concept of measurement and can be used as a basis. Environmental conditions have to be adapted and considered for measurement uncertainty evaluation separately for each measurement. It is important that the model for measurement uncertainty evaluation is validated and that the measurement is under statistical control.

The cause-and-effect diagram called the Ishikawa or fishbone-, diagram is quite a practical graphical tool that helps to visualize, and organize in a structured way the possible sources of uncertainty. Figure 5 demonstrates common components of an Ishikawa diagram for measurement uncertainty. The concept is to start with a horizontal arrow, the main bone. Direct influence quantities to the main bone are represented using new arrows pointing to the main bone and labeled with a name or description. This process can then be recursively iterated, adding new arrows or bones and refining the model as far as needed [13].

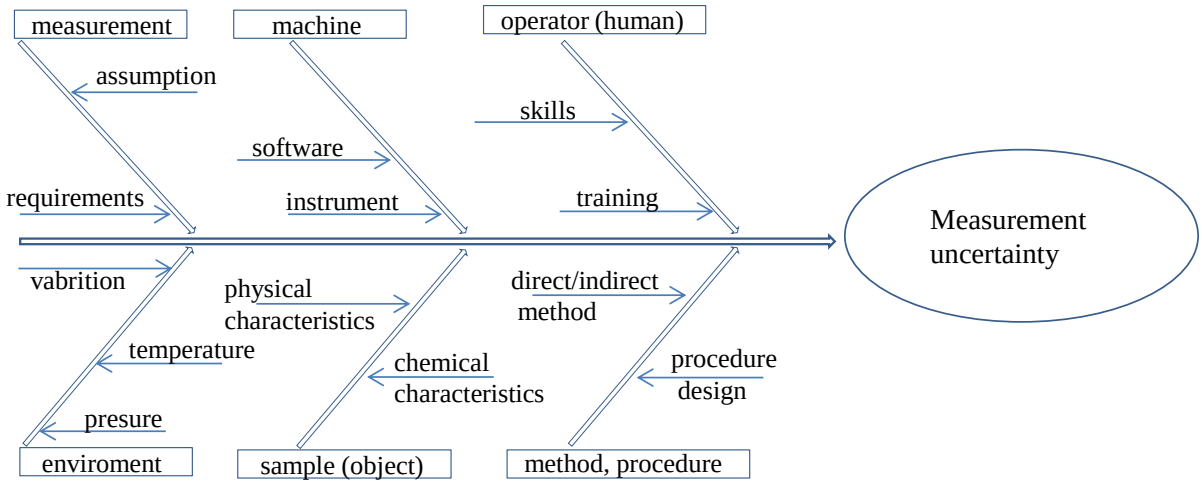

Figure 5: *General components that influence measurements uncertainty.*

After the identification of uncertainty sources the measurement uncertainty the mathematical model that describe their functional relationship need to be formulated.
GUM require a single (scalar) measurand Y to be described using the equation of the measurand,

$$Y = f(X_1; \ldots; X_N) = f(X) \qquad (1)$$

Where, the functional relationship f explains the mathematical dependencies of the distinct input quantities $X = (X_1; \ldots ; X_N)$. Each of the input quantities may be affected by an uncertainty and contributes to the measurement uncertainty of the specific measurement. The input quantities

$X_1; \ldots ; X_N$ can depend again on other influence quantities described with an additional functional relationship.[8] Standard uncertainty calculated for measurement function presented in equation 1 using Taylor series expansion described by equation 2:

$$u^2(y) = \sum_{i=1}^{N} c_i^2 \, u^2(x_i) = \sum_{i=1}^{N} u_i \, (y) \qquad (2)$$

Where, the best estimate of the output quantity Y defined as $y = f\,(x_1;\ldots;x_N)$ with N best estimates
$x_1;x_2;\ldots;x_N$ for the input quantities $X_1;\ldots;X_N$ that are described with appropriate probability distributions, $c_i = df/dXi$ – is partial derivate using of the f the best estimate x_i of influence quantities X_i usually called sensitivity coefficient.

In addition, if using the GUM approach, it is necessary to estimate the degrees of freedom to get an approximation for an uncertainty interval of confidence p for the measurand Y. The interval
$Y = y \pm U_p$ uses the expanded uncertainty $U_p = k_p u(y)$,
Where, the expansion factor $k_p = t_p(V_{eff})$ is taken from existing tables for t-distributions with V_{eff} degrees of freedom. The degrees of freedom can be calculated using the Welch-Satterthwaite formula [16]

$$V_{eff} = \frac{u^4(y)}{\sum_{i=1}^{N} \frac{u^4(y)}{v_i}}$$

Using the estimated variances $u^2(y)$ of Y and $u^2_i(y) = |c_i|u(x_i)$ of influence quantities X_i. The formula was originally thought for influence quantities of *Type A*, where we have explicitly v_i independent observations for analysis of an quantity X_i and, hence, the degrees of freedom $v_i = v_i\text{-}1$ for a quantity X_i are well defined.

However, it is not always obvious how to determine or estimate the degrees for *Type B* influence quantities, describing, for example, experience or expert knowledge.

The described framework for calculation of uncertainty has some limitation: first the information about probability distributions used to describe influence quantities uses only mean value and standard deviation, second is that the measurement model has to be linear or must be linearized for evaluation, which means that the measurement model is kept as simple as possible. To overcome those limitations Monte Carlo method has been suggested for uncertainty evaluation.

The first Supplement to the GUM has introduced a new approach for the evaluation of the measurement uncertainty. The final version of the document has been published in summer of 2008 after a lot of discussion and included the Monte Carlo method for measurement uncertainty evaluation [17]. This method has been used for measurements uncertainty evaluation by Couto et al. for complex measurement problem that could not be solved by GUM method [18]. In comparison between GUM and Monte Carlo methods have been found that Monte Carlo simulation had better results for a strong non-linear model. However, the limitations of the Monte Carlo simulation were the long runtime in complex cases; also the selection of the proper probability distribution function may be difficult [19].

The Monte Carlo method is a straightforward approach to calculate a discrete approximation G for the density function $G_Y(\eta)$ for the Equation 1 of the measurand Y with input quantities $X_1; \ldots ; X_N \in \boldsymbol{X}$ that contribute to the uncertainty of the measurand. Each input quantity is randomly varied according to the distribution function in M trials evaluating the equation of the measurand, so that with a large number of evaluations we get a large amount of possible values that can be attributed to the measurand Y according to the underlying model. Step- by-step procedure for evaluation of the measurement uncertainty using Monte Carlo simulation described in Supplement 1 to the GUM section 5.9.6.[13,17]

3 SURFACE CHARACTERIZATION

3.1 INTRODUCTION

As a response to demands created by industry in 2010 ISO published a series of standards regarding measurements of surface topography. Figure 6 interpreted from ISO 25178-6:2010 includes methods for measuring surface texture.

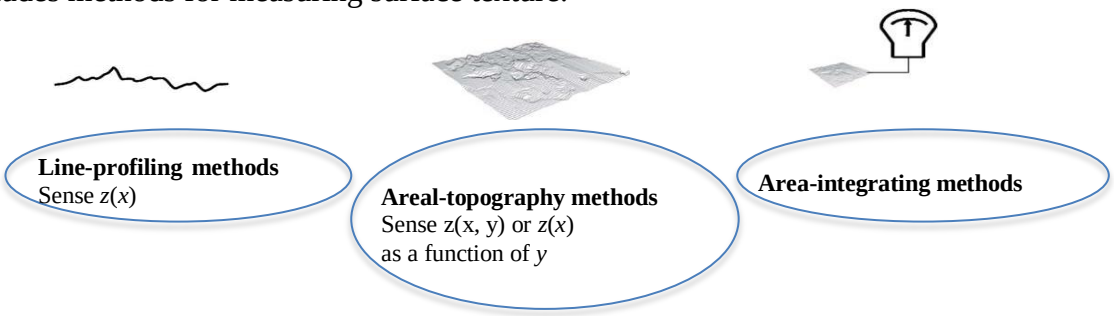

Figure 6: *A classification of surface texture measurement methods [20]*

Line-profiling methods provide information of the scanned profiles of examined surfaces and include the type of instruments based on: contact stylus scanning, phase-shifting interferometry, circular interferometric probing (scanning is circular so z is function of angle θ) and optical differential profiling. The 3D surface measurement is built from the series of profiles as demonstrated by Figure 7.

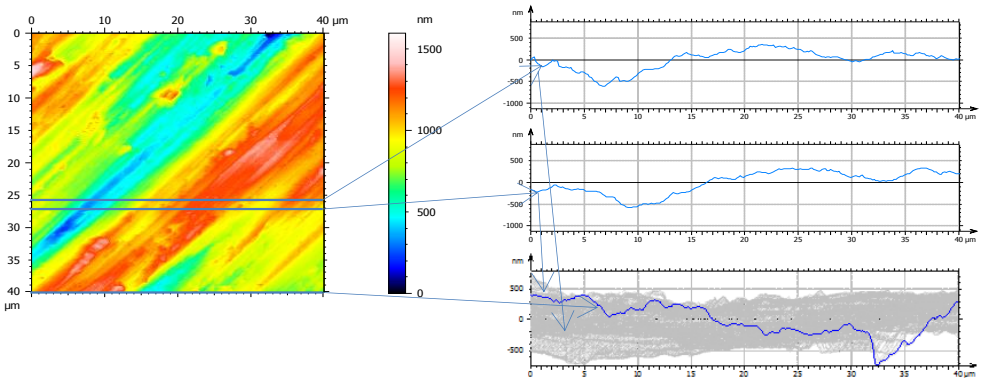

Figure 7: *Surface measurement performed by AFM (atomic force microscope).*

Areal-topography methods provide information of surface topography by producing topographic images *z(x,y),* or by producing the set of parallel profiles (*z(x)* as a function of *y*). Instruments that can provide this information are based on: contact stylus scanning, phase-shifting interferometry, coherence scanning interferometry, confocal microscopy, confocal chromatic microscopy, structured light projection, focus variation microscopy, digital holography microscopy, angle-resolved SEM, scanning tunneling microscopy, atomic force microscopy, optical differential profiling, point autofocus profiling.

Areal integrating methods are based on measurements that produce results dependent on area-integrated properties of surface topography. Usually these methods are used to perform repetitive surface texture assessments hence a calibrated specimen is used for comparison with the surface that is measured. Instruments based on this method are: total integrated scatter, angle-resolved scatter, parallel-plate capacitance, pneumatic.

3.2 MEASUREMENT TECHNIQUES

The instruments based on areal-topography methods can be divided into two groups: contact and noncontact profilers. In turn 3D instruments can be classified by the sensing method used to detect the surface texture. Figure 8 gives an overview of different groups of instruments according to the detection methods used for surface measurements.

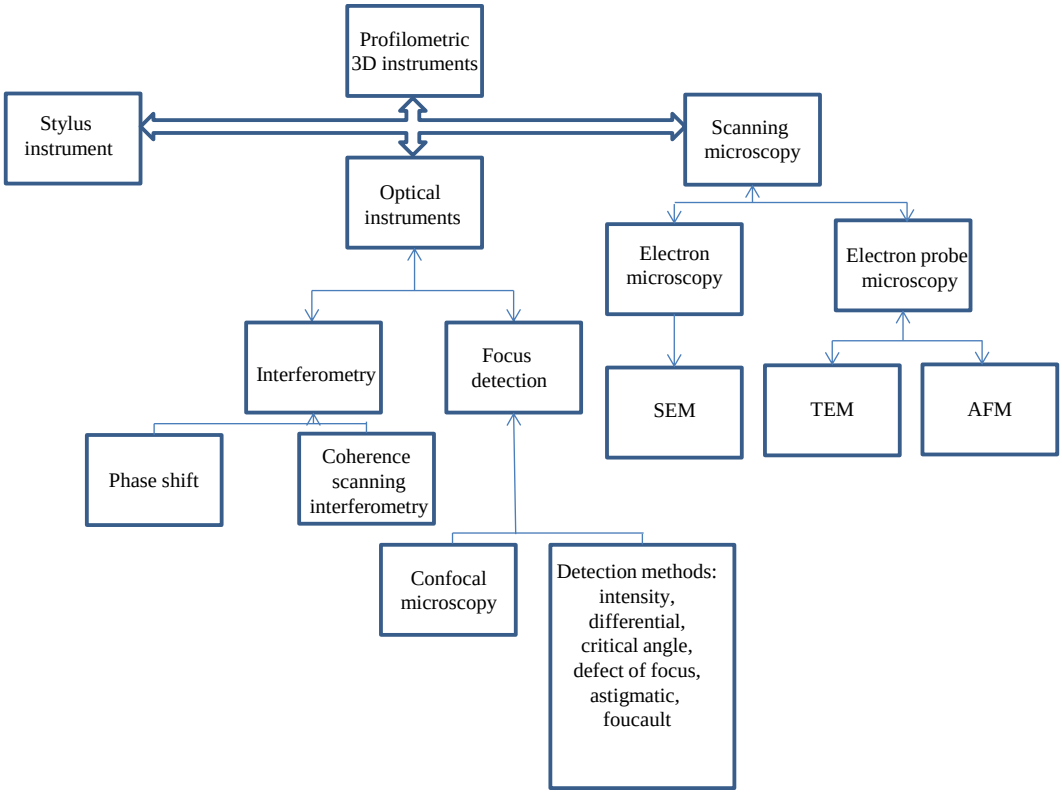

Figure 8: *A classification of profilometric 3D instruments based on sensing principle.*

3.2.1 CONTACT PROFILERS

The Stylus profiler is the most common technique that determines the surface characteristics via a stylus- based measurement system. The stylus is moved over the surface for a predefined distance. Its vertical movement relative to the datum is a measure of the deviation of the real surface from the geometrical surface. The stylus vertical movement is detected by a transducer such as a linear variable differential transformer (LVDT) and the corresponding recorded signal is converted into height data. By using an x-y-moving table most stylus instruments can provide 3D topography data. However measurement time increases drastically and can take hours, that is why these instruments are mostly used for profile measurements. The stylus tip is usually made of hard material such as diamond and has a radius of curvature in the range of 0,5-50µm. The vertical resolution of stylus instruments is determined by the stylus tip shape and radius of curvature, the lateral resolution of the instrument is defined by the sampling interval between the data points. The stylus radius and angle predefine the aspect ratio of the measured structures as well as the maximum slope that can be detected by the instrument. [21, 22, 23,24].

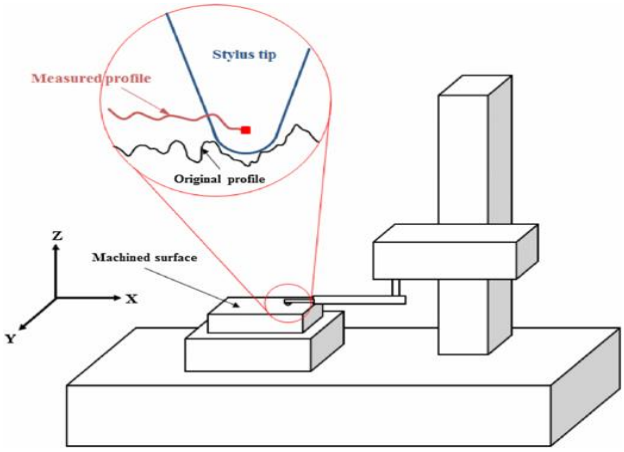

Figure 9: *Profile data acquisition by stylus profilometer [25].*

The stylus profiler can provide traceable measurements with high vertical (nm) and lateral (µm) resolution. However measurement speed, stylus tip sharpness and load applied to the stylus can cause surface deformation or lead to measurement error.

Scanning Probe Microscope

Another type of profiler is the scanning probe microscope (SPM). The measurements of surface micro structures and of surface local properties are performed by a very fine probe with a tip of size about ten nanometers or less. The distance between tip and measured surface in an SPM is about 0,1-10 nm. According to different types of interaction between tip and surface there are different types of microscope. For example tunneling microscope is based on the phenomenon of a tunneling current between a metal tip and conducting surface; various types of interaction forces are the bases for atomic force, magnetic force and electric force microscopes. [26]

Atomic Force Microscope (**AFM)**

The AFM is based on repulsive and attractive forces that occur between the tip of the AFM and the measured surface. Figure 10 illustrates the main components of an AFM to demonstrate the working principle and in practice is completed by a vibration system, computer and control devices. The AFM instrument includes a feedback system that keeps constant the interaction force between tip and sample, scanning elements that control the working distance between tip-sample and move the tip over the measuring surface, devices for precise control of the tip and sample position, and s vibration insulating system.

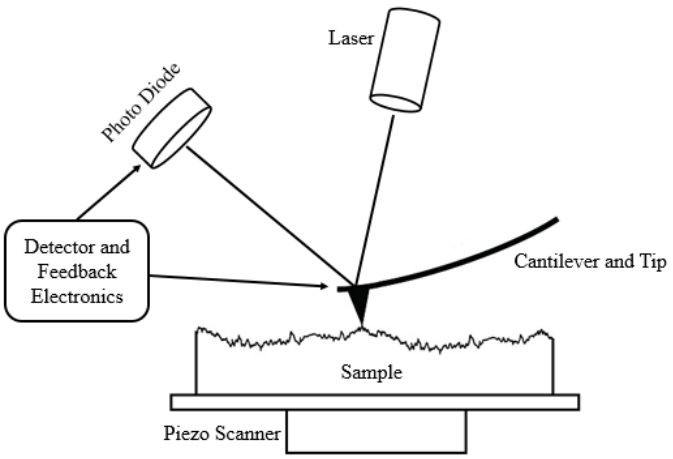

Figure 10: *Main components of Atomic Force Microscope.*

There are three different modes that characterize the working principles of an AFM: contact mode, non-contact mode and tapping mode. In contact mode the tip is in contact with the surface and as it scans forces between tip and surface cause the probe to bend. The surface information is obtained from deflection data. The deflection data can be measured by the laser signal reflected from the mirror placed on the probe (cantilever) or deflection can be monitored by a two-segmented photo diode in combination with a laser [27,28]. In contact mode the instrument is operated in a repulsive regime and constant force is applied to the tip under the scanning. When the height of the sample changes the tip will be deflected away from the set-point and the feedback loop will adjust the probe height using the scanner piezos to restore the probe bending to its original value (set-point). The possibility of detection of the lateral (or torsional) bending of the cantilever is useful for recording frictional maps of the imaged surface [29,30]. Measurements in contact mode apply to relatively smooth, hard surfaces. Measurements on soft surfaces create the problem when the probe is meeting step edges or from frictional and adhesive forces that can lead to damage to the surface or probe. In turn this leads to stick-slip movement of the probe and decrease in image resolution.
In the tapping mode cantilever oscillate at near to its resonance frequency close to the measured surface so the tip make repeatedly contact and disengages. Interaction between tip and surface is monitored by the oscillatory amplitude, which is restricted by increasing contact with sample. Height of tip is adjusted to keep the amplitude constant while the scanning of the surface is performed. In tipping mode observation of amplitude and phase signals is possible. Combination with information from height map may show surface features with better clarity. For example the phase signal is the difference between the oscillation and drive frequency and change when the probe move not only over different surface geometry but also affected by adhesive and mechanical properties of surface [31]. However the phase data is affected of the combination between different parameters such as: tip- sample adhesion, scan speed, load force, topography of sample it is difficult to extract quantitative information from phase map [32].
In addition to two previous modes AFM can operate in non-contact mode, then the cantilever is oscillated at smaller amplitude then in tapping mode. Then attractive or van der Waals and electrostatic forces occurs between tip and surface atoms occurs detectable shift infrequency of the cantilever oscillator. Adjusting the height of probe relative to the sample keeping this parameter stable under the scan allows building the height map of measured surface [33]. As no contact between tip and surface occurs under the measurements it allows very high atomic resolution under appropriate conditions [34]. It is still a technical challenge to achieve the atomic resolution using non-contact mode compare to tapping mode.

3.2.2 NONCONTACT PROFILERS

There are a number of advantages of non-contact profilers over contacting instruments: measurements can not cause any damage to the sample, measurement time is much shorter, and they are built to achieve 3D topography measurements. Usually the sample is illuminated with an electromagnetic wave and the response is obtained over the whole field of view, which allows information to be recorded much faster.
Electron microscopy is one of the noncontact techniques used for measurement of surface topography and can be divided into two types: Scanning Electron Microscopy (SEM) and Transmission Electron Microscopy (TEM)

A Scanning Electron Microscope (SEM) includes an electron optical column, vacuum system and signal detection and display elements. The electron optical column includes: an electron source (filament) to produce electrons; set of magnetic lenses to de-magnify the beam; magnetic coils to control and modify the beam; set of apertures to define the beam and

prevent electron spray. A vacuum system contains the chamber where vacuum is established; pumps to produce vacuum; valves to control vacuum and gauges to monitor it. Signal detection and display consists of detectors which collect the signal and electronics which produce an image from the signal. The drawback of the technique is that a non-conductive sample needs to be coated with conductive material for example gold to achieve the measurement image. SEM allows examination of the object using a magnification up to 100000 times with high lateral resolution, however the height of measured topography is presented in grey scale and no quantitative value is available. A stereo photogrammetry technique is used to create 3D topography from SEM images. Two surface structure images produced by SEM each at a differently inclined angle are condensed in an analyzing evaluation instrument where they overlap and create a three dimensional image.

Confocal microscopy

The confocal microscope has taken its name from the arrangement of the light path as the illumination and detection light paths share a common focal plane [35]. This is achieved by two pinholes placed at the same distance from the specimen, one in front of the light source and one in front of the detector, as shown schematically in Figure 11. Light goes through a pinhole in a beamsplitter (dichromatic mirror) to reach the objective and the specimen. At the same time the beamsplitter works as a filter which reflects the excitation wavelength but is transparent for all other wavelengths. Therefore the emitted light from the surface can pass through the beamsplitter to the detector. As a consequence of the pinhole arrangement, the detected light mostly comes from a narrow focal plane which improves the vertical resolution of confocal microscopes.

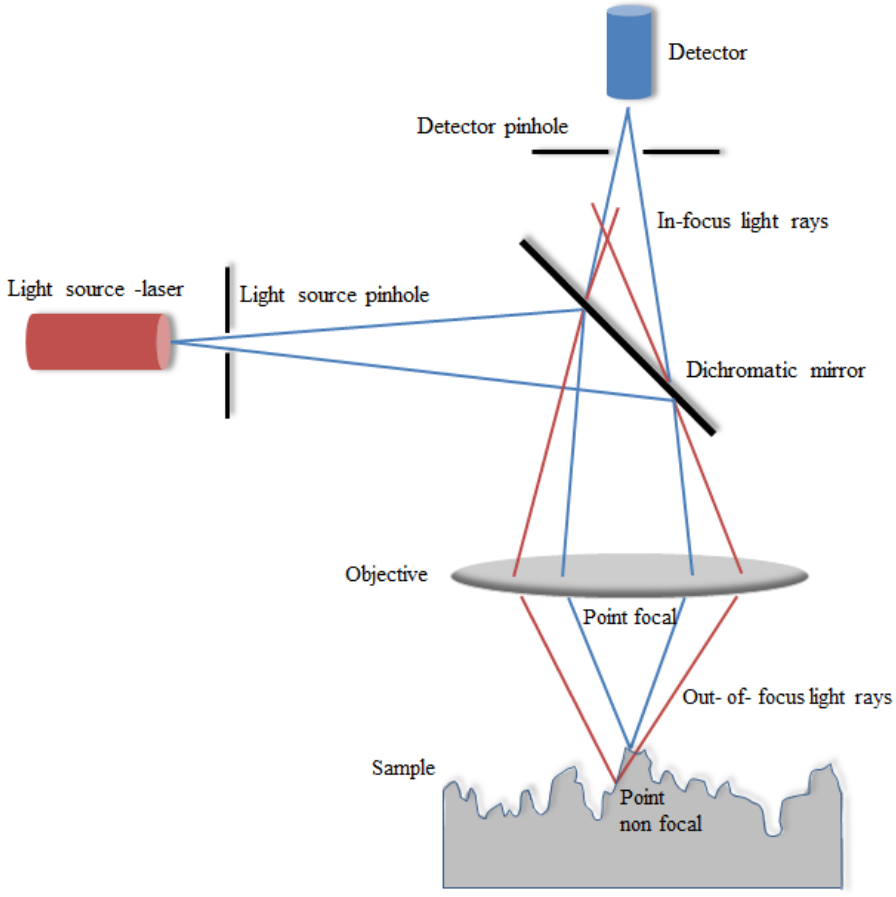

Figure 11: *Working principle of confocal microscope.*

There are two way of building the image by a confocal technique. Point-by-point scanning in x-y raster fashion results in a 2D irradiance image of the surface at the particular focus plane. Building of a 3D image requires either sample or objective or detector to be scanned vertically so each point of the surface passes through the focal plane of the microscope.[36] The benefits of confocal microscopy are: low signal-noise ratio; reduced blurring of the image from the light scattering; increased effective resolution. Over the years some improvements of data acquisition, modification of aperture and light source have been reported. [37,38,39]

Phase shift interferometry

Phase shift interferometry is based on the advantage of the wave properties of light to analyze the surface height variation. In PSI a time-varying phase shift is introduced between the reference wavefront and sample wavefront in the interferometer. By making more than three measurements of the irradiance of interference pattern as phase is varying it is possible to calculate the difference between the two interfering beams. The phase stepping is carried out at a constant rate as the detector is reading out the phase difference, while amplitude of the waves is kept constant under the PSI application. [40,41,42] The phase difference between two beams is usually achieved by changing the optical path by using the piezoelectric transducer to move the reference mirror by a fraction of a wavelength and respectively the phase is changed by a fraction of 2π.

The surface topography of the object is usually measured by sequentially shifting the phase of the reference beam by known amounts and measuring the resulting interference pattern. The relative surface heights are then calculated from the fringe data by different processing steps including an unwrapping algorithm to remove the phase ambiguities. PSI provides axial resolution in the nanometer to angstrom region with a lateral resolution in micrometers. These instruments are usually limited to the measurement of smooth polished homogeneous surfaces since measurement of rough surfaces with dissimilar optical properties introduces several errors in the measurement [43,44,45].

Coherence scanning interferometry (CSI)

CSI is the common name for a 3D measuring technique that combines the vertical resolution of an interferometer with the lateral resolution of a high powered microscope. There are several manes for techniques that use the same functional principles as CSI and White Light Interferometry (WLI) is one of them [46].

The CSI working principle has been presented by Davidson et al. (1987) [47]. The Linnik interferometer has been used to improve lateral resolution of measurement of smooth surfaces especially for semiconductors. The application of a Mirau interferometer in an optical profilometer has been reported by Bhusan et al in 1985.[48,49] In the same year Kino, Lee et al used a Michelson interferometer in a coherence scanning interferometer for surface height measurement [50].

White Light Interferometry uses the broadband illumination of a white light source and overcomes some limitations typical in single and even multiple-wavelength methods. The technique is widely used for measurements of engineering surfaces like MEMS devices, binary optics and machined surfaces. WLI does not involve phase shifting or complex algorithms, and is theoretically unlimited in the vertical scan length, which is only constrained by how far the reference mirror can move.

The drawbacks of an interferometer are that it cannot read discontinuities of the object geometry as in the case of sharp edges, and only works in relative coordinate space. These sharp edges can produce misleading diffraction spikes which can be mistaken for real peaks and thus can be a major problem in measurement interpretation.

3.3 CHARACTERIZATION METHODS

3.3.1 SURFACE ROUHNESS PARAMETERS

Characterization of surface topography is complex question. Profile characterization was standardized in the 1990s and is extensively accepted and used today [51]. In recent years 3D analysis has become a tool extremely practical and widely used for both industry and research. To assist in measuring of the engineering surfaces new ISO standards were established, but much work remains [52]. Earlier areal parameters have been a simple extrapolation of profile parameters. The tasks of the new standards are to define the contents of the areal surface texture standards, for specification and verification and to revise the profile standards to bring them in line with area standards. Table 3 shows the overview of surface area parameters.

Table 3: *Classification of surface roughness parameters.*

Family	Symbol	Parameters description
Height Parameters	S_q	Root mean square height
	S_{sk}	Skewness
	S_{ku}	Kurtosis
	S_p	Maximum peak height
	S_v	Maximum pit height
	S_z	Maximum height
	S_a	Arithmetical mean height
Spatial Parameters	S_{al}	Auto-correlation length
	S_{tr}	Texture-aspect ratio
	S_{td}	Texture direction
Hybrid Parameters	S_{dq}	Root mean square gradient of the scale limited surface
	S_{dr}	Developed interfacial area ratio of the scale limited surface
Feature Parameters	S_{pd}	Density of peaks
	S_{pc}	Arithmetic mean peak curvature
	S_{10z}	Ten point height
	S_{5p}	Five point peak height
	S_{5v}	Five point pit height
	S_{da}	Closed dale area
	S_{ha}	Closed hill area
	S_{dv}	Closed dale volume
	S_{hv}	Closed hill volume

Family	Symbol	Parameters description
Functional Stratified parameters	S_k	Kernel roughness depth (roughness depth of the core)
	S_{pk}	Reduced peak height (roughness depth of the peaks)
	S_{vk}	Reduced valley depth (roughness depth of the valleys)
	S_{mr1}	Upper material ratio
	S_{mr2}	Lower material ratio
	S_{vq}	Dale root mean square deviation
	S_{pq}	Plateau root mean square deviation
	S_{mq}	Material ratio
	$S_{mr\,(mc)}$	Areal material ratio of the scale-limited surface
	$S_{mc\,(mr)}$	Inverse areal material ratio of the scale-limited surface
Functional Volume Parameters	$V_{m(p)}$	Material volume
	$V_{v(p)}$	Void volume
	V_{mp}	Peak material volume of the scale limited surface
	V_{mc}	Core material volume of the scale limited surface
	V_{vc}	Core void volume of the scale limited surface
	V_{vv}	Pit void volume of the scale limited surface

Parameters defined in ISO 25178-2 have a prefix *S* or *V* the latter denoting volume parameters. They are divided on:

- height parameters is the class of surface parameters that quantify the z-axis perpendicular to the surface. Parameters included in this class are: S_q- root mean square height; S_a-arithmetic mean height;

S_{sk}- skewness is the third statistical moment, qualifying the symmetry of height distribution; S_{ku}- kurtosis fourth statistical moment qualifying the flatness of height distribution; S_p- maximum pick height; S_v- maximum pit height; S_z- maximum height of surface or height between highest pick and lowest valley.

-spatial parameters describe the topographic characteristics of the surface based on the spectral analysis. Parameters classified in this group are: S_{al}- auto correlation length or quantitative measure of the distance along the surface by which a texture statistically different from that at original location can be found; S_{tr}- texture aspect ratio is parameter that characterize the isotropy of the surface; S_{td} texture direction is calculated from the Fourier spectrum and shows in degree between 0° and 180° the main texture direction.

-hybrid parameters are characterizing a criterion depending on both amplitude and the spacing for example curvatures and slopes. S_{dq}-root mean square slope of the surface; S_{dr}-developed interfacial area ratio is used to measure the surface complexity, and useful in comparison of measurement under several stages of surface processing, and to find correlation in adhesion application [53] ; S_{td}- fractal dimension of surface.

-feature parameters belong to a new family of parameters. As features playing significant role in a specific application for example contact zone important to identify the features. S_{ds}-density of summits; S_{sc}-arithmetic mean summit curvature of surface parameters are useful for

characterization of surface glossiness. Parameters from this group find via segmentation and selected by a discrimination method called pruning.
-functional parameters are calculated from the Abbot-Firestone curve obtained by integration of height distribution on the measured surface. Usually distinguish functional stratified and volume parameter.
Functional stratified parameters are a class of surface finish parameters characterizing the functional aspect of a surface, particularly lubrication and grinding. They are the areal equivalent of functional profile parameters. Calculation of these parameters are based on a graphical construction of Abbot-Firestone curve over the surface, sometime the robust Gaussian filter can be applied before calculation of parameters. Parameters are mostly used by the automotive industry.
Functional volume parameters calculation is based on the Abbot-Firestone curve over surface using two bearing ratio thresholds that are defined by bearing ratios. Volume parameters are useful for evaluation of surfaces of mechanical components especially if components are used in contact with other surfaces. For example V_{vv} -pit void volume of the scale limited surface parameter uses to calculate the volume of fluid retention in the dip valley of surface and not affected by wear. V_{mp}-peak material volume of the scale limited surface parameter characterizes the volume of surface that will be removed during wear process.
Areal parameters give possibility to access the texture shape and direction; correctly estimate the surface features attribute and differentiate the connected and isolated features.

3.3.1.1 SPATIAL CHARACTERIZATION TECHNIQUES

The power spectral density function (PSDF), the autocorrelation function (ACF) and structure function (SF) are known as the spatial functions. These techniques offer a means of representing the properties of all wavelengths, or spatial sizes, of the features of surface texture; and are also called surface texture descriptors. The ACF of a random function is most directly interpreted as a measure of how well future values of the function can be predicted based on past observations. SF contains no more information than the ACF. The PSDF is interpreted as a measure of frequency distribution of the mean square value of the function that is the rate of change of the mean square value with frequency [54].
Advantages and disadvantages of the above listed techniques are presented in Figure 12 [1]

A: Excellent; B: Good; C: Medium; D: Poor

	Minimal Processing	Arbitrary Apertures	Apply to all Scales	Orthogonal	Connect to Performance	Intuitive -Design - Make
PSD	D	D	D	A	B	B
ACF	C	A	A	D	C	D
SF	A	A	A	D	C	B
Others						

Figure 12: *Quantitative evaluation of spatial content representations based on several criteria. (Figure interpreted from [1])*

3.3.1.2 POWER SPECTRAL DENSITY FUNCTION

Some years ago, the optics and the microelectronics communities encountered the need to deal more incisively with topography data [55-60]. It was found fruitful to Fourier transform the topography data to obtain the contribution at different lateral scales: the power spectral density (PSD). There has been a large number of studies dealing with PSD calculation from the topography data. Here the mathematical model of two-dimensional PSD calculation of a surface height map $h(x, y)$ is defined as [22, 59, 61]:

$$PSD(f_x, f_y) = \lim_{L\to\infty} \frac{1}{L^2} \left| \int_{-L/2}^{L/2} \int_{-L/2}^{L/2} h(x,y) e^{-2\pi i(f_x x + f_y y)} dx dy \right|^2, \quad (3)$$

Where, $h(x, y)$ is the surface topography data, and f_x and f_y are rectangular components of the surface frequencies. Eq. (3) describes the relative contributions of all the possible surface spatial frequencies for an ideal measurement of an infinite surface in the limiting case from zero frequency (an infinite surface) to an infinite frequency (infinitely small structure). In practice, topographic images of surfaces are recorded in the form of digitized data of surface heights, which is finite rather than infinite and sampled rather than continuous. For isotropic surfaces the PSD (f_x,f_y) function has polar symmetry, so the calculation of PSDs has been performed in polar coordinates:

$$f = \left(f_x^2 + f_y^2\right)^{1/2}$$

$$\alpha = tan^{-1}\left(\frac{f_x}{f_y}\right),$$

Averaging the resulting *PSD* (f,α) over the azimuthal angle yields the two-dimensional isotropic PSD:

$$PSD_{2D}(f) = \frac{1}{2\pi} \int_0^{2\pi} PSD(f, \alpha) d\alpha. \quad (4)$$

PSD functions describe two aspects of the surface roughness such as the spread of heights from

a mean plane, and the lateral distance over which the height variation occurs. The essential detail that needs to be taken into account for PSD measurement is the high-frequency content of signal allowed through the instrument as shown on Figure 13 below [62].

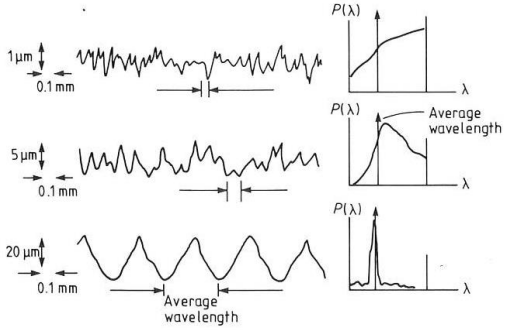

Figure 13: *Average wavelength and PSD. (Figure adapted from [62]).*

The PSD function has been widely used for characterization of optical surfaces but some limitations have been pointed out. Calculation of PSD is sensitive to data processing such as windowing and sub-aperture choosing. Different calculation techniques may lead to different results [63].

3.3.1.3 AUTOCORRELATION FUNCTION

The ACF was first used in surface metrology by J. R. Womersley and M. R. Hopkins in 1945 [64], but it was J. Peklenik [65] who used the ACF in terms of a typology for surfaces. Later the other approach the discrete technique, was originated by Whitehouse [66,67] who, with J. F. Archard derived a functional significance from the distance over which it decays.

The autocorrelation function is a powerful tool for characterization of surface topography.

The definition of autocorrelation function is:

$$A(\tau) = E[z_1, z_2] = \lim_{L\to\infty} \frac{1}{L} \int_{-L/2}^{L/2} z(x) z(x+\tau) dx \quad (5)$$

Where, z_1, z_2 are the two measurements taken on the surface a distance τ apart, *E[]* is the expected value of the product of these two measurements over all the surface. Two conditions should be satisfied for correct application of equation (5): first the random nature of surface is uniform in distribution and the second the ergodic theorem which states that the time average of a function along the trajectories exists almost everywhere and is related to the space average, holds. The ergodicity for a surface means that averages of many profiles taken at the same time or *x* value are the same as averages taken of one record over all time.
An important property of the ACF is that it can be linked to the "average machining unit event". Whitehouse applied the ACF to analysis of the grinding process. Figure 14 shows how the shape of ACF can relate to the machining process. The randomness of the process (how the grains are distributed in the wheel surface) determines the envelope of the ACF of the surface texture. The shape of the grains and how each grain interacts with the surface will determine the fine detail of the ACF as shown in Figure 14 [68].

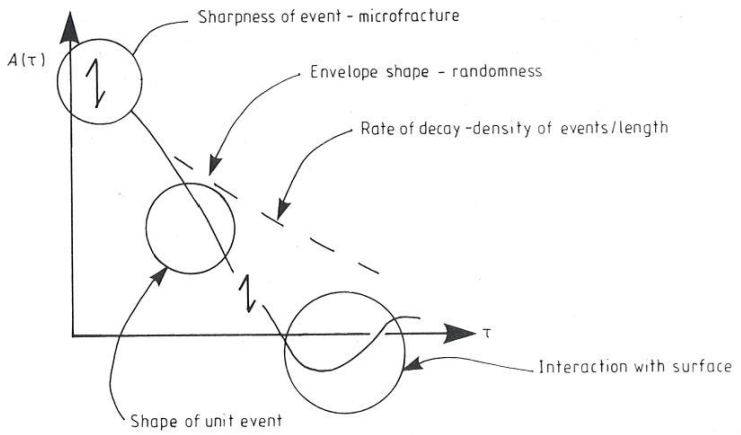

Figure14: *Relation of ACF shape to process. (Figure adapted from [68]).*

3.3.1.4 SURFACE STRUCTURE FUNCTION

The structure function can be used as complement for the PSD and ACF techniques. It was introduced by Kolmogorov in 1941 for the analysis of statistical problem in turbulence theory [69,70]. Later it was used for characterization of machined surfaces [71], optical surfaces [72,73], in turbulent flow fields[69,70,74], for time series analysis in astronomy [75,76].
The linear SF can be calculated from both profile data and areal data.
The SF was first introduced in surface metrology (for profile data) in D. J. Whitehouse's PhD thesis [77] in 1971,

$$S(\tau) = E_1[z(x) - z(x+\tau)]^2 \qquad (5)$$

Where, E_1 is the statistical expectation of the squared height difference as function of separation, of $z(x)$ that represent height position at x and $z(x+\tau)$ is the height a distance τ away from x.

4 COHERENCE SCANNING INTERFEROMETRY (CSI)

4.1 INTRODUCTION

A number of surface texture parameters can be estimated from topography data. However, the parameter values depend on the method used for the measurement. Areal- topography methods include information of the spatial resolution and the sampling length in each direction which allow to easily calculating surface parameters.
An example of a non-contact optical measuring technique is a coherence scanning interferometry. This technique will be discussed in the following section.

4.2 FORMATION OF WHITE LIGHT FRINGES

Coherence scanning interferometry (CSI) plays a central role in noncontact strategies for process development and quality control. It provides customers with full 3D measurement of surface characteristics that influence the functional behavior of manufactured parts. A brief review of principles of this technique is described in section 4.3.
While CSI is certainly not new, combining white light interferometry techniques with modem electronics, computers, and software has produced extremely powerful measurement tools. A technical advantage is that it uses the broad spectral band of a white light source, with wavelength from about 380 up to 750 nanometer.[78,79] As known from the theory of light white light is a combination of different wavelength and provides a larger measurement range than laser sources. Another important phenomenon used in coherence scanning interferometry is interference. It is caused by the superposition of two electromagnetic waves. When two waves are in phase they create constructive interference or bright bands on an interference picture and when two waves are out of phase they create destructive interference or dark bands. Figure 15 illustrates the interference fringes creation.

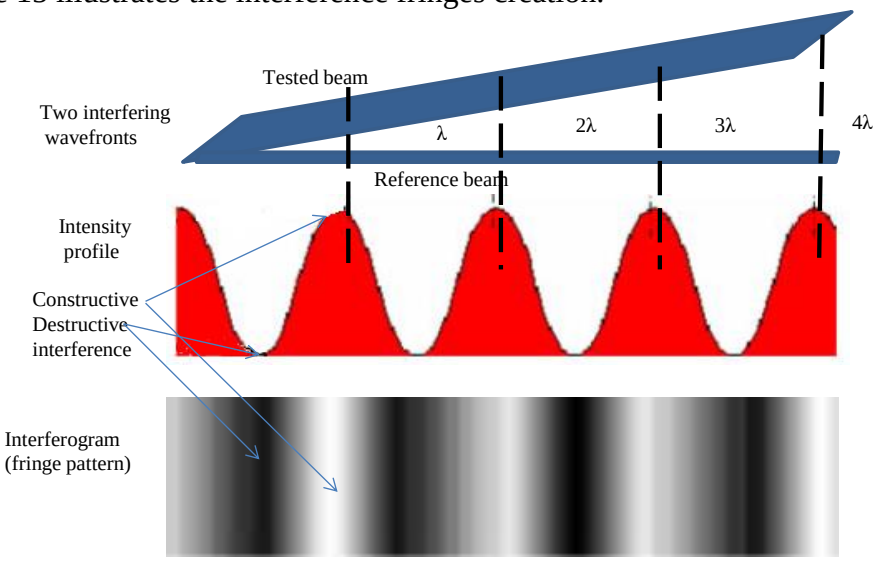

Figure 15: *Interference fringes creation.*

Mathematical representation of inference is described by the equation

$$I=I_1 + I_2 + 2\sqrt{I_1 I_2}\cos(\varphi_2 - \varphi_1), \qquad (6)$$

Where, I_1 and I_2 are the intensities of two waves, the component $2\sqrt{I_1 I_2}\cos(\varphi_2 - \varphi_1)$ is the interference term and $(\varphi_2 - \varphi_1)$ is the phase difference between waves.[80] The phase difference can be directly related to the OPD (optical path difference):

$$OPD = \left(\frac{\lambda}{2\pi}\right)(\varphi_2 - \varphi_1), \qquad (7)$$

The highest contrast of fringes is obtained when the position of the reference mirror is at the best focus of the objective, so that the OPD (optical path difference) is zero. Due to the large spectral bandwidth of the light source, the coherence length of the source is short and allows the appearance of contrast fringes when the two paths of interferometer match in length.

4.3 WORKING PRINCIPLES

Figure 16 shows the key features of an automated interference microscope enabled for CSI, where the left side of the Figure is showing a white light interferometer built at Halmstad University. The main components of the instrument are: piezo drive system (piezo motor), digital image sensor (CCD camera), broadband light source, interferometric objective, optical components (system of lens and beam splitters), data acquisition firmware and computer control. Data acquisition involves the continuous motion of the piezo drive system that moves the interferometric objective along the z-axis, which in turn synchronizes the scan of focus and optical path length. The optical path length is defined as the product of the distance the light travels through the systems and the refractive index of the medium it travels. As mentioned earlier when the difference between the optical path lengths for the two waves is zero interferometric fringes are obtained. Interferometry is dependent on the light source used. The most common are: tungsten-halogen, incandescent or arc lamp. More often a white light emitting diode (LED) adapted into the Köhler illuminator is used today [81]. Cameras that can be used for visible wavelength in a CSI setup are usually of CCD (charge coupled device) or CMOS (complementary metal oxide semiconductor) type. The CCD and CMOS are developed to convert light into electric charge and process it into electronic signals. Difference is in how the pixel charge is proceeding until it transferred in signal. Camera selection involves not only field size and number of pixels but also the acquisition speed, response linearity, quantum well depth, digitization resolution, and the ability to shutter electronically [82].

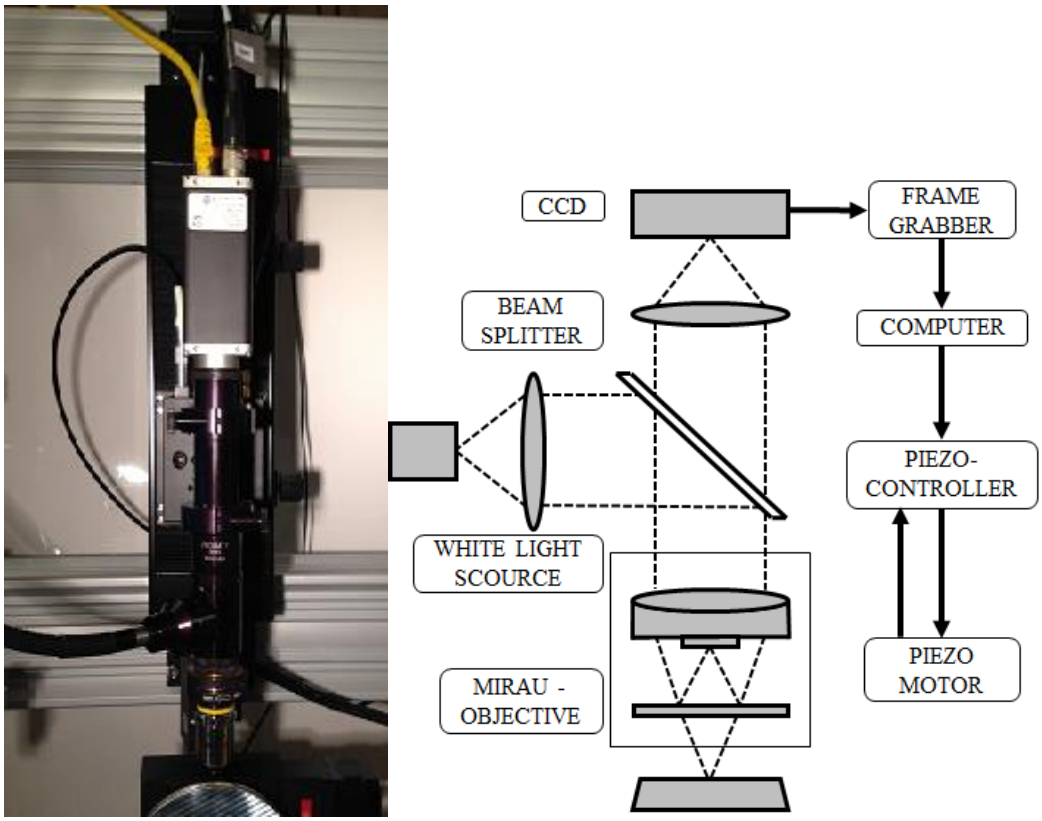

Figure 16: *Key components of Coherence Scanning Interferometer.*

4.4 INTERFERENCE OBJECTIVES

The most common interferometric objectives used in CSI are shown in Figure 17: Mirau, Michelson and Linnik objectives. Choice of objectives is directly linked to the surface to be measured, working distance and magnification of objectives.

The Michelson interferometric objective is suitable for measurements where applied magnification can be low, working distance is long and numerical aperture is low. It is built so that the beam splitter cube is placed under the objective lens and the reference mirror is placed on the side. The Mirau objective is suitable for higher magnification measurements and short working distance. It consists of two thin glass plates, the lower glass plate works as a beam splitter and the plate above includes the reference mirror. The Linnik interferometer was developed to overcome the problem with magnification linked to the previous described objectives. It is built of two identical bright-field objectives with a beam splitter in between. This objective can be a solution for systems that require high magnification, high numerical aperture objectives and a short working distance that could not include a beam splitter. It can be used when a long working distance is needed to admit large samples to be measured. Table 4 presents the relation between magnifications of objective, numerical aperture, working distance and lateral resolution [84].

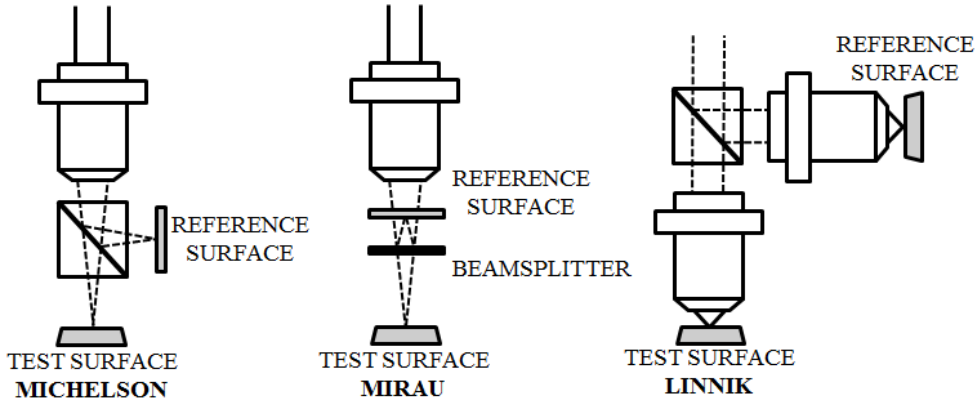

Figure 17: *Interferometric objectives represented schematically. (Figure adapted from [83]).*

Table 4: *Interferometric objectives and their optical characteristics.*

Objective type	Magnification	NA (numerical apeture)	Lateral resolution (Raleigh criterion) (µm)	Working distance (µm)
Wide field *	0,5x	0,015	17,2	40
Michelson	1x	0,03	8,62	40
Michelson	2,5x	0,08	3,45	40
Michelson	5x	0,13	1,99	40
Michelson	10x	0,28	0,92	18
Mirau	10x	0,3	0,86	7,4
Mirau	20x	0,4	0,65	4,7
Mirau	50x	0,55	0,47	3,4
Mirau	100x	0,85	0,3	0,5

*wide field objective ref[81]

The numerical aperture of objectives is the measure of its ability to gather the light to resolve the sample details at a fixed object distance. Numerical aperture was defined by Abbe as the sine of the half aperture angle multiplied by the refractive index of the medium between the objective front lens and the sample:

$$NA = n \sin\theta \qquad (8)$$

Where, *n*-refractive index of medium (*n*=1 for air that most typically is medium) and

$$\theta = \arctan(P/f)$$

Where, *P* is pupil radius and *f* -focal length.

Parameters related to optical properties of objectives and some parameters related to surface slopes and high-spatial-frequency changes contribute to limitation of lateral resolution of interference objectives and later whole CSI.

Lateral resolution of an instrument is defined as the smallest distance between two features that can be detected [85]. Theoretically lateral resolution of optical system can be given by the Raleigh criterion:

$$r = 0{,}61\frac{\lambda}{NA} \qquad (9)$$

Where, λ is the mean wavelength of the light source and NA is the numerical aperture of the objective. Another measure of lateral resolution can be given by the Sparrow criterion that defines spatial wavelength for which the instrument response drops to zero. For this criterion the factor 0.61in eq. 9 is replaced by 0.82. Both criterions should be checked to determine the minimum lateral resolution of CSI. For some instruments the distance between the pixels in the camera may determine the lateral resolution.

In context of determination lateral resolution of CSI as the ability of an instrument to measure the spacing between the points on the image together with the ability to determine the height of features on the surface, the lateral resolution is defined as one-half the spatial period of a sinusoidal profile for which the instrument response falls to 50%. The instrument response can be measured from instrument transfer function which is the analog of modulation transfer function for topography [86,87].

4.5 SIGNAL FORMATION FOR SURFACE RECONSTRUCTION

In CSI surface topography is obtained from intensity data recorded for an individual pixel as a function of scan position. The localization of interference fringes allows the determination of the height of the sample surface by identification of the scan position that corresponds to the frame of the highest contrast fringe at each pixel. Figure 18 shows the signal modeling in Mirau objective.

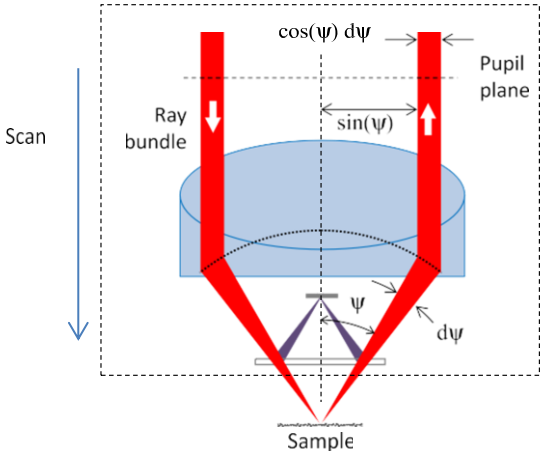

Figure 18: *Schematic of signal detection in Mirau objective. Adapted from ref [88]*

Mathematical description of signal modeling for CSI is described further below.
Interference fringes frequency is described by the equation

$$K(\beta, k) = 2k\beta$$

Where, $\beta = \cos(\psi)$ is directional cosine and $k = {}^{2\pi}/_{\lambda}$ the angular wavenumber for the specific wavelength λ.

The interference signal described by the one ray bundle at the incident angle that correspond to the specific point of image is

$$g(\beta, k, \zeta) = 1 + cos[-K(\beta, k)\zeta + \phi(\beta, k)]$$

Where, ϕ is phase value

$$\phi(\beta, k) = K(\beta, k)h + \varpi((\beta, k)$$

h-height of surface and ϖ-offset of CSI optical system parts.

Incoherent superposition include sum of interference contribution $g(\beta, k, \zeta)$ over angular wavenumbers k, weighted by illumination and detection spectrum V(k) and over all directional cosine β weighted by distribution of light in pupil U(β)

$$I(\zeta) = \int_0^{\infty} \int_0^{1} g(\beta, k, \zeta)\, U(\beta)\, V(k) \beta d\beta dk$$

The imaging system sums the individual interference contribution over the pupil. Integration over all points in the pupil create the net signal that can be described as an inverse Fourier transform of the frequency spectrum

$$I(\zeta) = \int_{-\infty}^{+\infty} q(K) \exp(-iK\zeta)\, dK \qquad (10)$$

Where, non-zero positive part of the frequency spectrum is

$$q(K) = \rho(K) \exp(-iKh) \qquad (11)$$

In this equation the surface height of interest enters as a phase term *Kh*. The frequency spectrum can be calculated using integration over all wavenumbers $k = {}^{2\pi}/_{\lambda}$ in the source spectrum.

$$\rho(K) = \int_{k={}^{K}/_{2}}^{\infty} \sqrt{R_{ref} R}\, \exp(i\gamma)\, U[\beta(K, k)] V(k) K/4k^2 dk$$

Where, *R*- object intensity reflectivity, R*ref* -is reference reflectivity including mirror and beam- splitter, V(k) –is the effective source spectrum, including the transmissivity of the optical components and camera sensitivity, directional cosine β is coupled to the wavelength as $\beta = \frac{K}{2k}$,
and $\gamma = \upsilon - \omega$ where υ- is the phase shift coupled to the reference path, and ω- is coupled to measurement path. [81]
Equation (10) gives the qualitative understanding of the signal generation process and Figure 11shows graphically creation of incoherent superposition model. Generally the WLI signal can be represent as intensity scan *I(ζ)* or the Fourier frequency spectrum *q(K)* with components of Fourier spectrum calculated from incoherent superposition model.

4.6 SIGNAL PROCESSING

Envelope detection

The surface height is obtained either by the modulation envelope, the phase estimation of interference fringes or a combination of both.

The recorded system intensity are qualitatively characterizes by interference fringes and overall variation in signal, which links the interference effect to specific position of scan $h_{x,y}$-ζ At a given pixel position, the intensity can be written as $I_{x,y}$

$$I_{x,y}(\zeta) = I_0(\zeta) + I_{AC}(\zeta - h_{x,y})\cos\left[K_0(\zeta - h_{x,y})\right] \quad (12)$$

Separated in two parts $I_0(\zeta)$ - constant offset and co-sinusoidal function of signal at a frequency *Ko*, and I_{AC} is modulation envelop function.

The equation (12) describes the signal envelop concept using envelop-modulated carrier and corresponds to idealized condition.

Envelope and phase estimation in frequency domain

The main drawback of the envelope detection technique is that it sensitive to error sources such as optical aberration, diffraction, noise and vibration. The combination of envelope detection and phase estimation is used to improve the measurement outcome. The problem with this combination is that envelope detection usually performs in scan domain, then phase modulation in frequency domain, to overcome this problem entire signal transforms to frequency domain via Fourier transform. The Figure 19 [81] shows the relationship between scan and frequency domain. The high-resolution surface topography map for x,y-pixel can be described:

$$h_{x,y} = \frac{\theta_{x,y}}{K_0} + \frac{2\pi}{K_0} round\left(\frac{A_{x,y} - \langle A\rangle}{2\pi}\right)$$

Where,

$$A_{x,y} = \theta_{x,y} - K_0 H_{x,y}$$

is the phase gap between two analysis results, the round function returns the nearest integer to its argument and the $\langle A\rangle$ represent the field average. The phase gap in frequency domain describes as and shown in lower part of Figure 12

$$A_{x,y} = intercept\left[arg\left(q_{x,y}(K)\right)\right]$$

and first estimate of surface high topography map that is a line fit to the argument $q_{x,y}(K)$as range of function over frequency range K

$$H_{x,y} = slope\left[\arg(q_{x,y}(K))\right]$$

$q_{x,y}(K)$ as seen earlier nonzero positive portion of frequency spectrum regain from intensity map via Fast-Fourier transform.

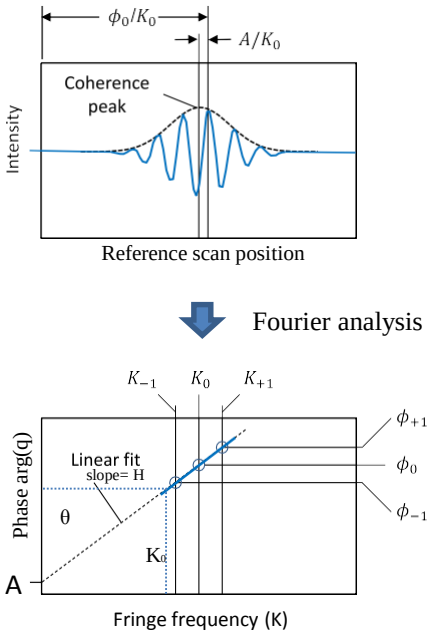

Figure 19: *Representation of envelop modulation in frequency domain. Adapted from ref[81]*

Scan domain

An alternative method to detect envelope and phase of intensity data $I_{x,y}(\zeta)$ in each pixel is to correlate it to complex kernel that describe the CSI signal.

The symmetric complex kernel can be described:

$$f_{z'} = c_{z'} + is_{z'}$$

Where $c_{z'}$ is the real and $s_{z'}$ imaginary coefficients.

From PSI (phase shift interferometry) algorithm the kernel coefficients can be used for CSI cases. Coefficients correspond to the 5 points data that describe the envelope per fringe and reads:

c=(0 2 0 -2 0)

s=(-1 0 2 0 -1)

The envelop detection can be described by common terms as:

$$S_{x,y}(\zeta) = \int_0^{\infty} f(\zeta')I_{x,y}(\zeta + \zeta')d\zeta'$$

or in discrete form as

$$S_{x,y,z} = \sum_{z'=-N/2}^{N'/2} f_{z'}I_{x,y,z+z'}$$

Where, $f_{z'}$ is complex kernel. Using the kernel coefficient the envelop reads as:

$$|S_z| = \sqrt{(2I_{z-1} - 2I_{z+1})^2 + (-I_{z-2} + 2I_z - I_{z+2})^2}$$

and phase reads as:

$$\phi = \tan^{-1}\left(\frac{2I_{z_{0-1}} + 2I_{z_{0+1}}}{-I_{z_{0-2}} + 2I_{z_0} - I_{z_{0+2}}}\right.$$

Centroiding

An alternative method for signal processing is using the centroid. Idea is to estimate the overall signal position of the square of signal derivative.[89] This techniques does not required the phase information to acquire the measurement and can be described as:

$$H = \frac{\sum_z (I_z - I_{z-1})^2 \, \zeta_z}{\sum_z (I_z - I_{z-1})^2}$$

Where, z is frame number.

4.7 SURFACE MEASUREMENTS PROBLEM

Transparent film

The ability to distinguish multiple reflections from semi-transparent film structures has been detected in 1990 [90]. Transparent films are used in anti-reflection coatings, mirrors, semiconductor and flat panel display industry and designed to control the amount of light reflected or transmitted at a surface for a given wavelength.

Transparent film has the thickness comparable to the illumination wavelength and affects the amplification coefficient on z. The main task in analyzing film thickness map is to identify the modulation envelopes corresponding to surface reflection from the film boundaries. As the secondary surface signal or signal from substrate usually is influenced by axial group velocity optical path length, which is longer in film than in air and the position of best focus which is shorter in film than in air. The Figure 20 shows the film thickness analysis for CSI [91].

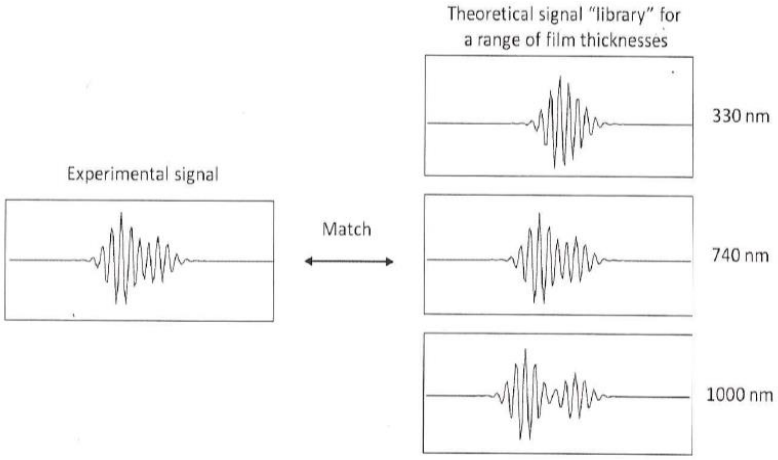

Figure 20: *Analysis of film thickness for CSI. Adapted from [91]*

Dissimilar materials

Optically dissimilar materials have a significantly different Fresnel phase change on reflection. Such phase changes leads to errors in height variation measurements performed by CSI across boundaries of different materials if the "optical phase change on reflection" varies across such boundaries. Under the measurement when light is reflected from the specularly reflected object surface it interferes with light in an interferometers reference beam. The modulation of fringes depends on the complex index of refraction of the surface materials. The complex index of refraction is given by the term n_c =n-ik, where *n* is the real part that indicates the amount of deflection of a ray of light passing through the material, and *k* is the imaginary part that indicates the amount of absorption. The error occurs when measuring the objects surface with two or more dissimilar materials in the same field of view. While the variation in measured height is accurate within each area of a particular material, an error in measured height occurs across boundaries between dissimilar materials within the field of view due to the above-mentioned different phase change on reflection [92].

5 CALIBRATION PROCEDURE OF WHITE LIGHT INTERFEROMETER

5.1 INTRODUCTION

The demand from high precision technologies led to a need of high accuracy in non-contact techniques that CSI can satisfy. However CSI is still slowly accepted in production due to the lack of standardization and missing comparability to tactile methods. So far no accepted standardized solutions exist for determination of measurement uncertainty. Figure 5 shows that one of the components that affects the measurements uncertainty is the contribution from the measurement machine. The aim of calibration and traceability for the measurement instrument is to provide the confidence that the measurement result is of reliable quality. The calibration procedure includes the testing mechanism that allows comparison of the measurement result performed by the instrument with another verified measurement method. This process in turn provides an unbroken link to the primary standard in our case the metre, which defines the traceability of instrument. [93,94]

The setup of the instrument plays an important role for achieving the reliable results of measurements. In turn all parts of the setup affect the metrological characteristics and the measurement uncertainty of a white light interferometer [93]. The Ishikawa diagram (Figure 21) shows the influence of the instrument components on the metrological characteristics for surface texture methods.

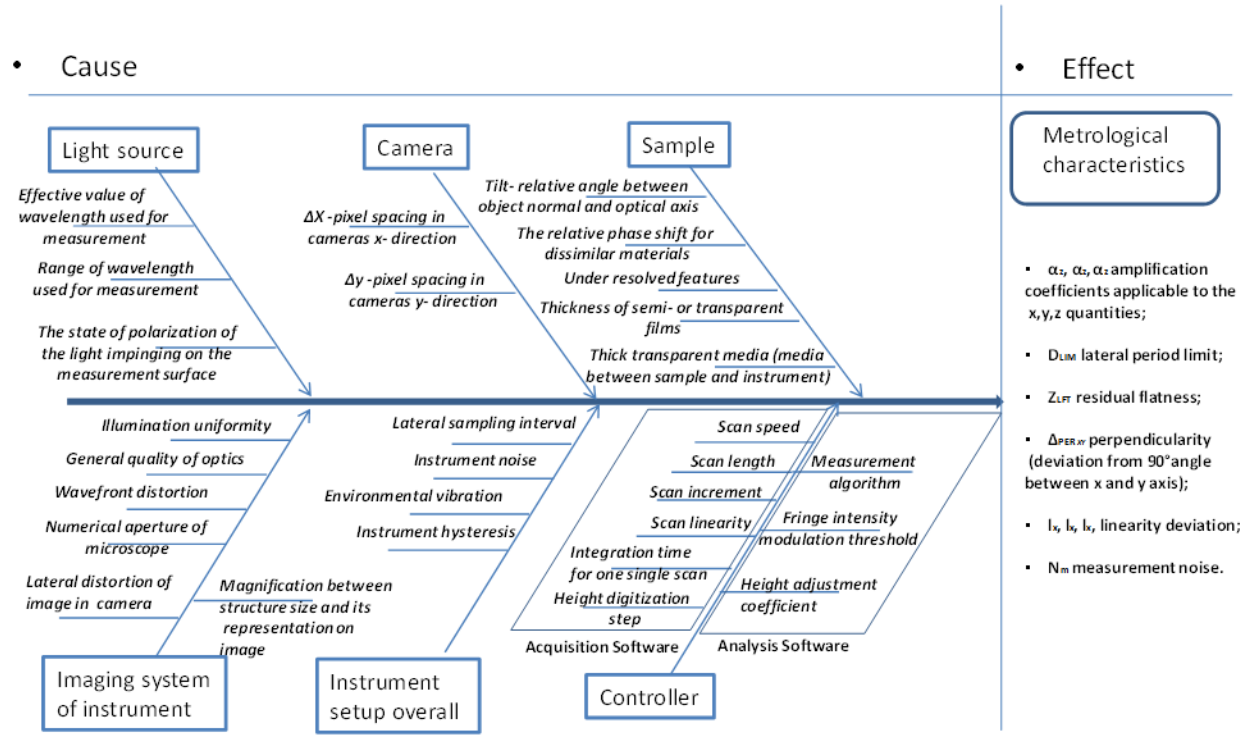

Figure 21: *Influence of coherence scanning interferometer components on metrological characteristics of measurement.*

The Light source by emitting the proper span of wavelengths in a specific spectral band affects the amplification coefficients of the instrument. The amplification coefficient is defined as the slope of the linear regression curve obtained from the response curve. The response curve is the graphical representation of the function that describes the relation between actual and measured value. Figure 22 shows that the maximum linearity error corresponds to the maximum deviation of the instrument response curve from the linear curve and the amplification coefficient is the slope of the linear curve.

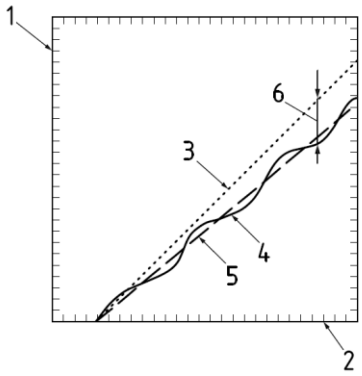

Figure 22: *An example of linear response curve for the instrument. 1 measured quantities, 2 input quantities, 3 ideal response curve, 4 response curve, 5 linear curve [95].*

Cameras format ranging or pixel quantities affect the lateral period limit of the instrument. The lateral period limit is the spatial period of a sinusoidal profile when the instrument's response falls to 50%. This metrological characteristic is directly linked to the ability of the instrument to resolve the closely spaced features, and to the lateral and spatial resolution of the instrument. The spatial resolution of an optical system is defined by the Rayleigh criterion, or the Sparrow criterion. The Rayleigh criterion can be used to find the instrument response to features much less than the mean wavelength of the light source. The Sparrow criterion defines when the instrument response falls to zero.

Sample condition and shape have an impact on amplification coefficients of measurement. Relative angle between the surface normal and optical axis of the instrument affect the amplification coefficient for x, y and z- quantities. In the literature the cases with high slope on the surface have been studied and differences in results performed by different measurement techniques have been reported [96]. The explanation is that the light reflects at or near to the edge of the numerical aperture of the objective and causes signal loss.

The imaging system influences most of the metrological characteristics of measurement. Uniformity of illumination under the measurement over the field of view of the object affects the amplification coefficients, linearity deviation (l_x,l_y,l_z) and flatness of the areal reference (Z_{FLT}). The quality of the optics that includes aberration, transmission, alignment error have an impact on the lateral period limit (D_{LIM}), and perpendicularity (Δ_{PERxy}) of the system in addition to metrological characteristics listed earlier. Wavefront distortion is the function that describes deviation in the measured optical path from deviation in both the reference and measured arms. This parameter influences the amplification coefficient for z. Numerical aperture, as it usually depends on the wavelength of light affects amplification coefficients and lateral period limit. Lateral distortion of the image affects the lateral capability of the instrument, and if a surface has significant slopes the errors can be introduced into measurement of heights. [97] This parameter influences residual flatness, lateral period limit, perpendicularity, linearity deviation and amplification coefficient for x and y quantities. Magnification between object feature size and its size on the image sensor concerns the amplification coefficients for x and y value.

Instrument overall refers to the influences from the instrument noise, instrument hysteresis, environmental vibration and characteristics linked to lateral sampling interval. The measurement noise is common known metrological characteristics that occurs during the use of instrument and includes the instrument noise. The instrument noise is the internal signal added to the measurement caused by instrument if it placed in noise-free environment, or it means the noise from electronic components of instrument. Instrument hysteresis influences the linearity deviation. The linearity deviation is the maximum local difference between the line from which the amplification coefficient is derived and the response curve. The lateral

sampling interval influences the lateral period limit of instrument which is equivalent to the spatial period of sinusoidal profile at which the height response of instrument falls to 50%. Environmental vibration is the mechanical motions that disturb the CSI scan in an unpredictable and unwanted way, that cause measurement errors.

The controller in CSI has two functions: one is to perform acquisition of measurement and the second is to analyze the data for correct result presentation. The acquisition and analysis software influences the amplification coefficient and linearity deviation linked to z movement such as scan speed, scan length, scan increment and scan linearity. The CSI behaves like a highly parallel optical contact probe and the software records the location of the CSI signal at each pixel with respect to a scan position, resulting in a surface topography map, the scale and linearity of which are directly linked to the capacity of the scan motion. The time required to complete a single scan and the digitization step or variation between two ordinates extracted from the surface affect the measurement noise that in turn contribute to measurement uncertainty.

Further on the calibration of metrological characteristics listed in Figure 21 will be examined in order to find their contribution to the standard and combined uncertainty.

5.2 INSTRUMENT NOISE DETERMINATION

There are many factors that contribute to the noise in CSI measurements. Vibration, photon noise, CCD noise, quantization and motor error are some of them and combination of these factors creates two types of noise: static and dynamic (or measurement noise), that can be measured in practice.[98]

The static noise is usually linked to electrical noise and environmental vibration. The static noise is not significant in case of calibration of instrument scales as it is part of measurement noise.

The measurement noise limits the capability of the instrument to measure the features of high spacial frequency. The measurement noise can be isolated from measurements on an optical flat with flatness deviation less than 30nm. There are two techniques for determination of noise contribution in measurements: the subtraction and averaging. The subtraction method uses two measurements at the same position on the sample performed over a short period of time. The noise value can afterwards be calculated as $S_{q\ noise}$

$$S_{q\ noise} = {Sq}\Big/{\sqrt{2}}$$

S_q –root-mean-square value of standard deviation in units of height from statistics over full image of surface point, and is calculated as difference between two measurements.

Averaging method based on assumption that noise contribution decrease for repeated measurements performed at the same place on flat. The S_q value is the function of the $S_{q\ noise}$ and $S_{q\ flat}$ and describes as:

$$S_q = \sqrt{{S_{q\ flat}}^2 + {S_{q\ noise}}^2}$$

After *n*-repeated measurements the contribution of instrument noise can be calculated as:

$$S_{q\ noise} = \sqrt{\frac{n}{n-1}\left(S_q^2 - S_{q_n}^2\right)}$$

Noise value achieved by two methods shows no significant difference. [99]

Figure 23 demonstrates practical application of the subtraction method for determination of noise level for the commercial coherence scanning interferometer MicroMax. Measurements 1 and 2 are taken directly after each other and the result of subtraction shows the noise level that will be encountered in measurement results produced by the instrument.

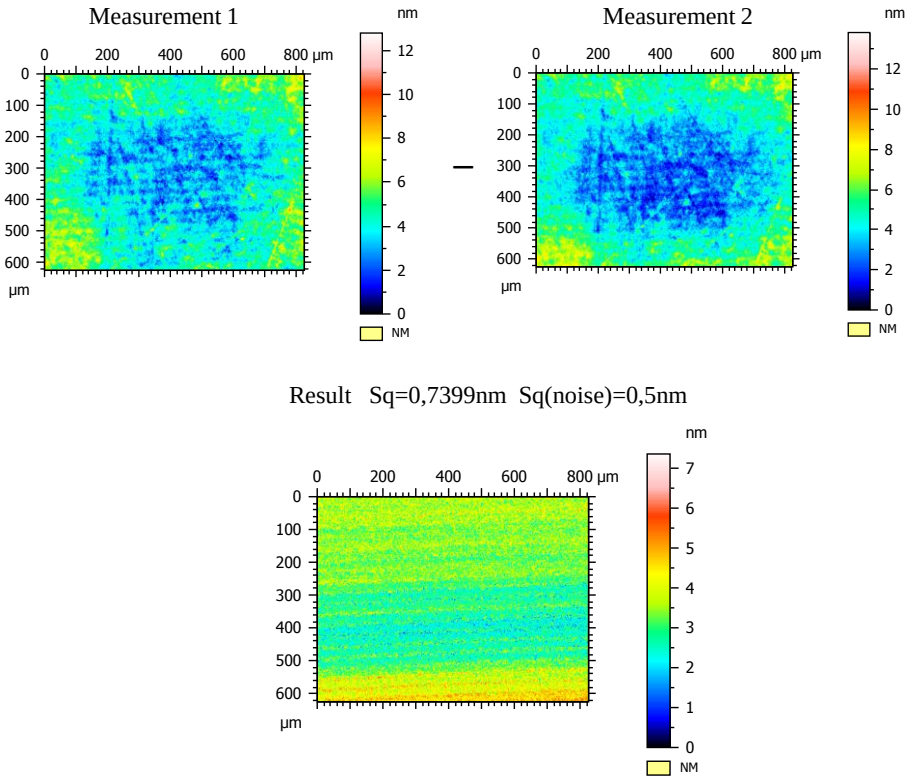

Figure 23: *Flow-chart for subtraction method for noise determination.*

5.3 FLATNESS DEVIATION OF AREAL REFERENCE

The flatness deviation of its areal reference is a factor that affects the metrological properties of a white light interferometer. In scanning instruments surface topography measurements rely on the quality of interference objectives' reference. Topography measurement performs against the areal reference of interference objectives and any flatness deviation of the reference will result in an error in z- axis measurements direction.

Determination of the flatness deviation of an areal reference can be achieved by applying the average method to measurement of a standard optical flat. The residual flatness of a CSI can be determined by using an averaging method, accordingly to VDI/VDE 2655 [100], by averaging ten measurements performed on different places on a standard flat. The value of S_z (maximum height) parameter is used for this purpose. This parameter is calculated as the sum of the maximum value of peak heights (S_p) and the maximum value of valley depths (S_v) on the surface within the measured area. As a standard flat surface used for measurements is not perfect and usually scratches and debris are observed on its surface filtering and outliers removal techniques need to be applied to achieve useful measurement results. The threshold method in combination with a polynomial filter of 12th order as recommended by Giusca et.all [99] has been applied to determine the residual flatness of the instrument. The threshold value for surface peak height (S_p) and valley depth (S_v) was determined as three times the S_q value of the measured flat surface. The sequence of data modification is shown in Figure 24.

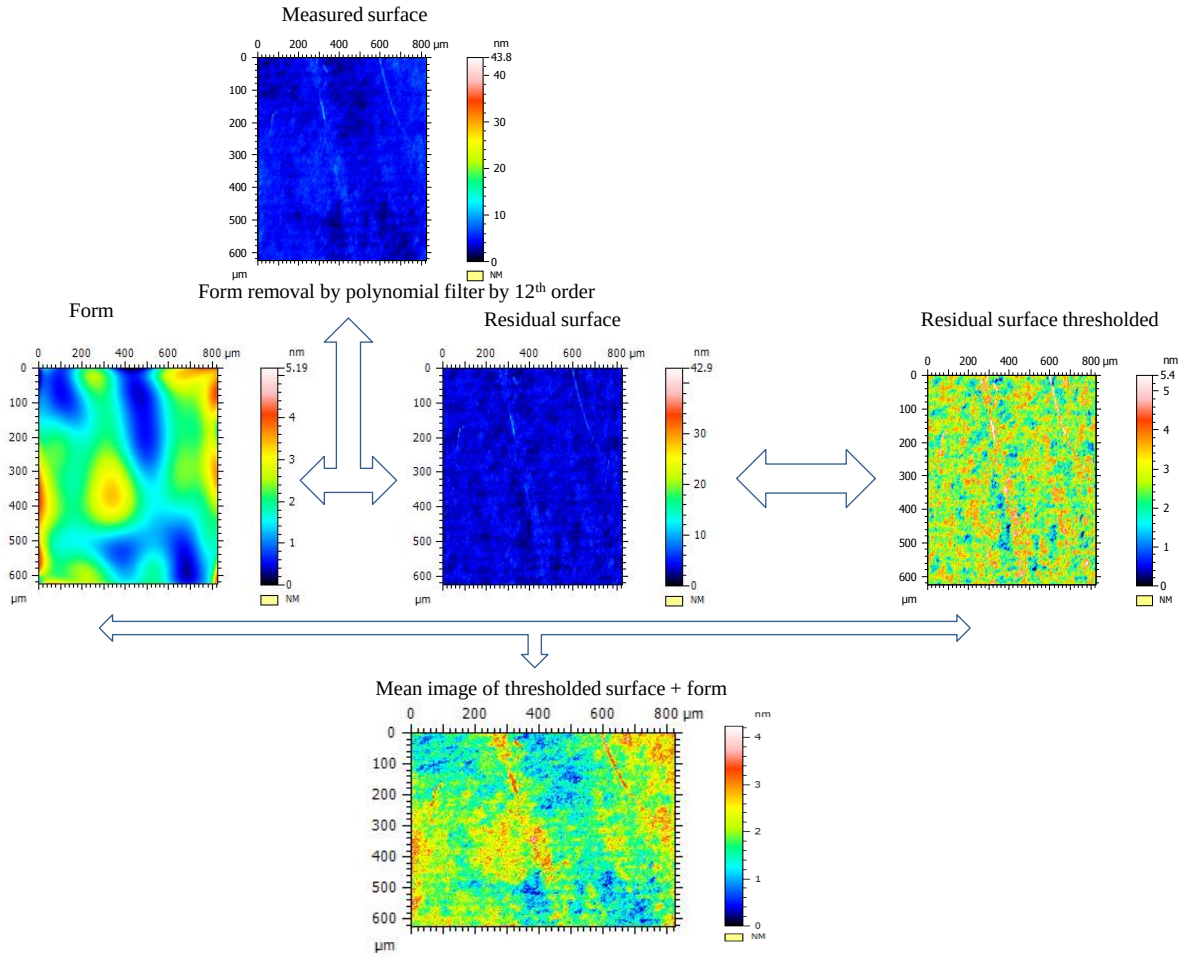

Figure 24: *Flow-chart include sequences of data modification for evaluation of reference flatness of instrument.*

5.4 AXIAL CALIBRATION

5.4.1 Z-AXIS CALIBRATION

The aim of z-axis calibration is to estimate such metrological characteristics of instrument as the z amplification coefficient (α_z) and linearity error (l_z) listed in Figure 21. The calibration procedure includes a series of measurements performed on step height standard artefacts with different height. For the calculation of amplification coefficient it needs to establish the relationship between the ideal response curve and the instrument response curve demonstrated on Figure 22.

The set of step height standards that cover the whole z working range of the instrument or at least the set that covers the most used range of measurement is required to perform the calibration.

The amplification coefficient can be established from the equation:

$$\alpha = \frac{\sum_i^n C_i I_i}{\sum_i^n C_i^2}$$

Where, α is an amplification coefficient, C_i is the calibrated value, I_i is indicated value and n is the number of height step standards used for measurements.

There is no standardized procedure for areal measurement of step height. The existing method for profile measurement of the height of a step height is described by ISO 5436 standard [101]. In our case the artefact that includes six grooves with increasing depth from 0,275µm to 9,41µm has been used for measurements. The groove height has been calculating according

to ISO 5436. A mean line representing the upper level was drawn over the groove and the depth was assessed from the upper mean line to the lowest point of the groove. The groove analysis is presented graphically in Figure 25. The profile in the centre of the figure has been extracted from the areal measurement above, and groove depth has been determined as shown in the lower profile according to ISO analysis.

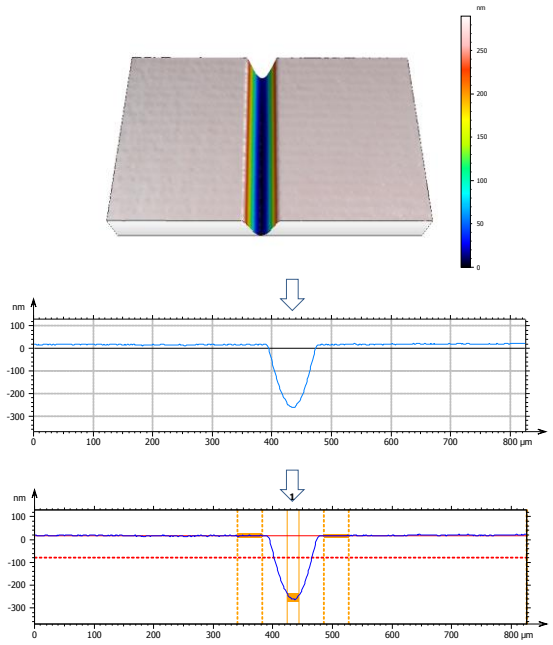

Figure 25: *Flow-chart of the groove standard analysis.*

The vertical range of the calibrated instrument is 100µm. For determination of repeatability and reproducibility of the CSI, measurements of groove height have been made in five positions within the range of the instrument (at 10%, 30%, 50%, 70% and 90% of CSI working range).

Repeatability is an indication of the variation in repeat measurements made on the same subject by the same instrument under identical conditions. This means that measurements are made by the same operator if human input is required by the same method or equipment under the same environmental conditions in a short period of time so the result value will be considered constant. Variability of the measurements in a repeatability process can then be ascribed to errors due to the measurement process

Reproducibility is an indication of the variation in measurements made on the subject under changing conditions. This means that measurements can be made by different instruments and different observers over a period of time and changing of the environmental conditions needs to be taken into account.

5.4.2 X AND Y-AXIS CALIBRATION

As well as z-axis calibration, x and y-axis calibration is required for estimation of amplification coefficients (α_x, α_y) and linearity errors (l_x, l_y) for x and y-axes of the CSI. Another metrological characteristic that needs to be estimated is the x,y axis perpendicularity (Δ_{per}). For this purpose different type of artifacts are available, two of which are shown on Figure 26: a cross grating artifact (type ACG), and a NPL ODS (Optical Dimensional Standard).

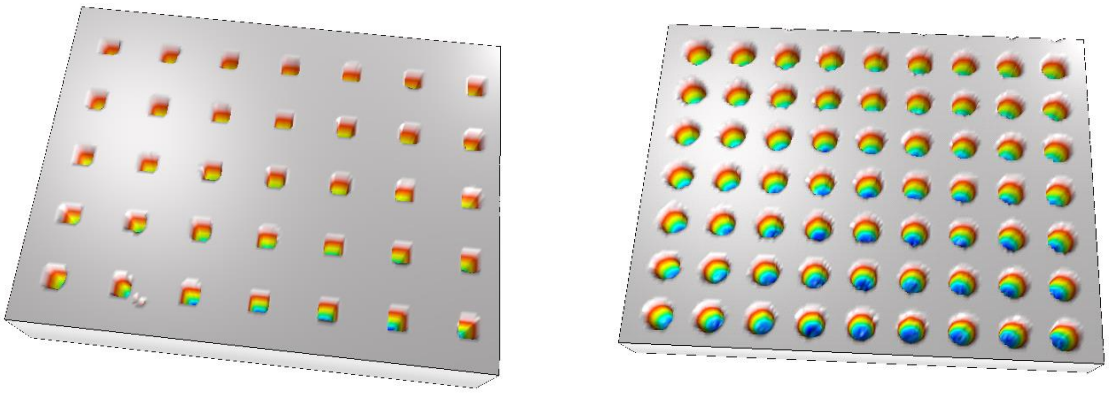

Figure 26: *Overview of standards: type ACG artifact-left; NPL ODS (Optical Dimensional Standard) –right.*

For the determination of amplification coefficients and linearity error the position of the centre of gravity of the pore on ACG artifact or the centre of circle of the hole for the NPL ODS artifact can be used. In both cases the position of centre of gravity of pore or centre of circle of hole can be calculated using image processing that will not take into account the height of pores or holes. The axis perpendicularity can be calculated as the angle between two nominally orthogonal rows.
In this study for x,y scale calibration of the CSI an NPL ODS artifact with a 75 μm pitch has been used in 10x magnification lens configuration and for 50x magnification an artifact with 15 μm pitch. Under the measurements the rows of holes of NPL ODS were oriented as parallel as possible to the x and y axis of the instrument. The 5° misalignment between the artifacts axis and instrument axis will not have any significant effect on measurement uncertainty.[102] As in the case with z-scale, calibration measurement of artifacts have been performed only once on five positions (10%,30%,50%,70%,90% of working range) distributed over the vertical range of the instrument.

5.5 RESOLUTION

5.5.1 DEFINITION OF LATERAL PERIOD LIMIT AND INSTRUMENT TRANSFER FUNCTION

It need to be clarified that z-axis resolution and x,y-axis resolution for CSI are determined separately. The measurement noise includes the z-axis resolution, and the lateral period limit is used to estimate the x and y-resolutions of the CSI. According to the ISO/CD 2013 the lateral period limit is *a special period of a sinusoidal profile at which the height response of an instrument falls to 50%.* This definition is related to the linear system theory. However the lateral period limit does not only depend on the properties of the instrument but also on the measured surface structure. As it is pointed out in the literature the lateral period limit has to be measured within the linear height range of the instrument, otherwise the instrument's result is unpredictable due to a nonlinear response.
Usually the lateral resolution of an optical system is described by the number that expresses the smallest separation between features that can be distinguished on the image. This description corresponds to the optical resolution of the imaging system represented by the Rayleigh criterion $r = 0{,}61\frac{\lambda}{NA}$ or the more generous Sparrow criterion $r = 0{,}47\frac{\lambda}{NA}$ previously described in chapter 4.4. It needs to be pointed out that optical resolution is the smallest centre-to centre feature separation on the measuring object, not the smallest or thinnest object that can be seen.

The CSI measurements differ from those of a 2D imaging system, since two points on a height profile corresponding to different height levels need to be separated. Figure 20 shows the difference between the optical resolution of a CSI and the lateral resolution of a microscopic imaging system.
According to VDI/VDE guideline 2655-1.1 [95] the short cut-off wavelength of a CSI can be two or three times the optical resolution because of the diffraction limit. In order to take advantage of the diffraction-limited resolution, the camera pixel size in object space must be smaller than *r*, otherwise the resolution is camera-limited. For some CSIs camera resolution matches the optical resolution up to approximately 10X, meaning that the pixel size in object space has the same lateral dimensions as listed in Table4 chapter 4.4.
ISO 25178-604:2013 includes the method for lateral resolving power of CSI using Instrument Transfer Function (ITF). As amplitude transfer characteristics of instrument cannot be calculated from optical resolution limit de Groot et al. defined an "Instrument Transfer Function (IFT)". The IFT is based on the "Modulation Transfer Function (MTF)" and known from imaging system theory. The ITF shows the response of the CSI as a function of the objects spatial frequency component, of course the ITF is the function of the spatial frequency of the sinusoidal object. The validation of ITF requires measurement of the instruments response over the range of spatial frequency. The artifact for ITF measurements can include an assortment of sinusoidal grating patterns. Another method is to measure the profile of a sharp step feature. A step height generates a continuum of spatial frequencies for comparison with the known step profile using the Fourier transform ratio at each spatial frequency. [103,87] There are number of cautions regarding the ITF: one is that it is theoretically valid only for surface heights much smaller than the wavelength, second is that higher spatial frequencies can cause errors in the results, third the features with larger height variations can have unexpected results, including sensitivity to spatial frequencies beyond the Sparrow criterion, because of nonlinear coupling. [86]

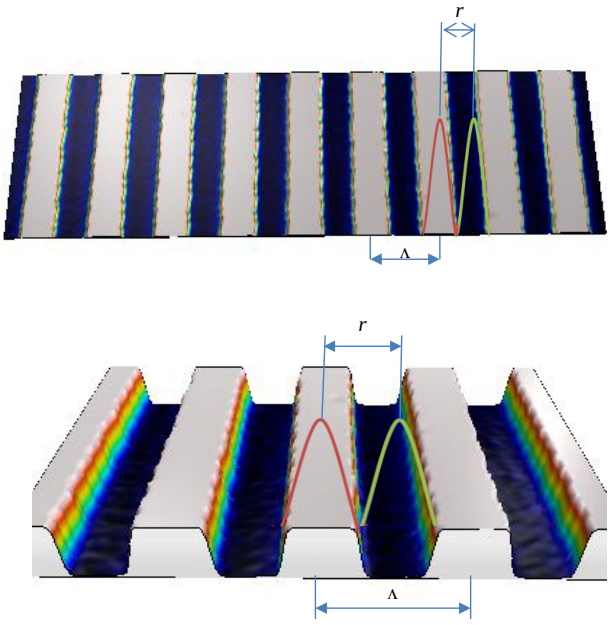

Figure 27: *Lateral resolution (Rayleigh criterion) in microscopic imaging where a 2D amplitude grating of period Λ is resolved (top), and in 3D CSI measurement resolving different height levels of a grating structure of period Λ (bottom).*

5.5.2 DETERMINATION OF LATERAL PERIOD LIMIT

For determination of lateral resolution limit of CSI the multiple grids of different pitches can be used. As long as the pitch of gratings are smaller than resolution of instrument no height information can be measured, only than the pitch increase instrument start to resolve the height of the grating.

The Siemens star is usually used for two-dimensional microscopy for determination of lateral resolution of optical systems. The ASG standard is based on the Siemens star principle but developed for 3D optical instrument for estimation of lateral period limit of instrument. The advantage of ASG standard is to use the star pattern for extraction of profile along the radial direction of the star.[105] For the determination of lateral period limit of CSI two profiles needs to be extracted from the star pattern. Figure 28 demonstrate the two profiles extracted through the centre of two diametrically opposite raised (left part of Figure 28) and lowered petals (right part of Figure 28). The profile resulting from subtraction of those two profiles calls Instrument Response Profile (IRP) and will be the base for determination of the lateral resolution of CSI. In ideal situation the edges of profile should have the value of petal height and the central part should be zero, the area where the height difference drop due to the limited lateral resolution is the area of interest for determination of lateral period limit of instrument. Some modifications need to be done with IRP before determination of resolution can be performed. First the vertical scale of profile need to be normalized to the maximum height value, second the horizontal scale of profile need to be recalculated using the equation: $Lx = \frac{\pi}{180} n°$, where n is the angle in ° of the star pattern petals. The equation is the simple modification of length of circle arc formula. After the lateral period limit can be determined from IRP profile accordingly to ISO by measuring the width of the central depression at 50% height.

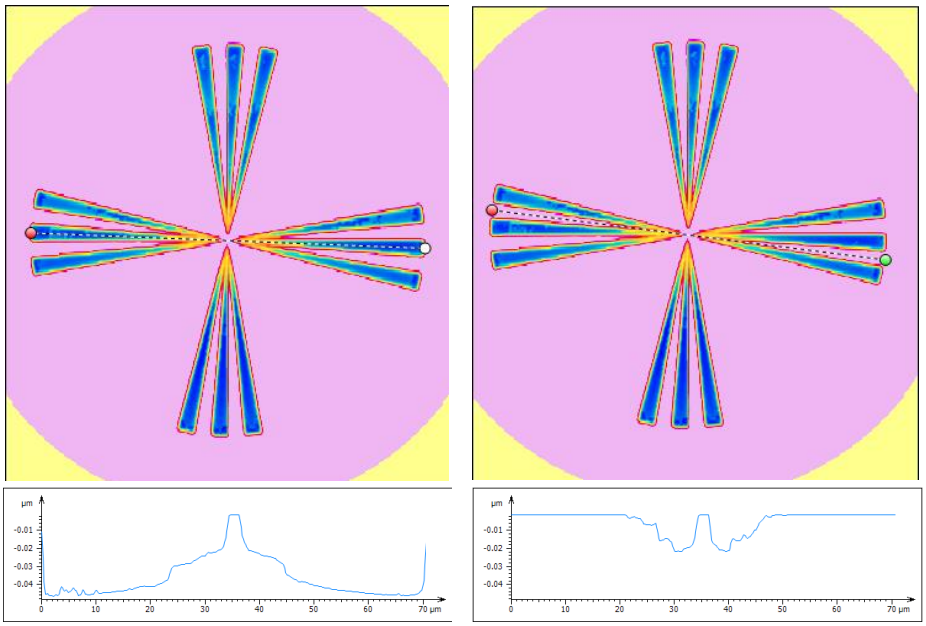

Figure 28: *The example of the extraction of two profiles from ASG standard star pattern.*

Left side of figure shows the place and profile extraction performed on the two opposite lowered petals passing through the centre of the star pattern. Right side of figure shows the similar extraction of profile but performed on the upper petals of star pattern.

The Figure 29 shows steps after the subtraction of profiles extracted from the upper and lowered petals has been done. The first profile is result of subtraction in next profile the

normalization of the x and z scales are applied: z- height =100% and x-scale = value achieved from the equation mentioned earlier. The last profile shows the value of lateral period limit at 50% height of z-scale.

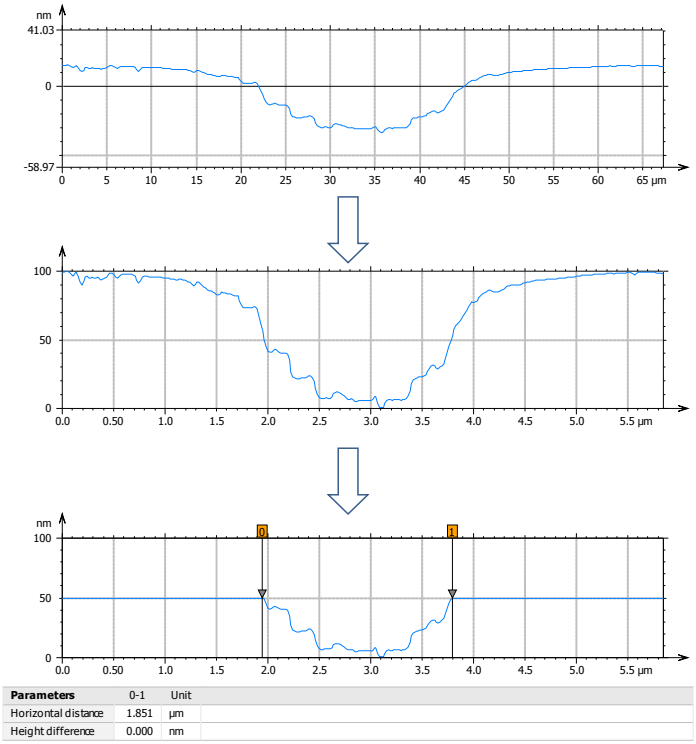

Figure 29: *Example of determination the lateral period limit of the CSI.*

The figure 30 shows the step-by-step flow for the determination of lateral period limit of the CSI.

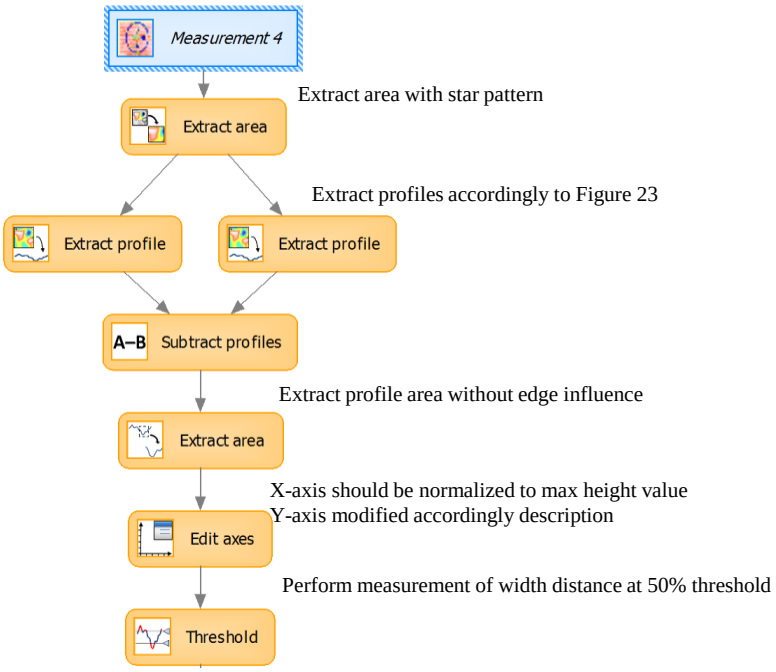

Figure 30: *Flowchart for the determination of lateral period limit of CSI.*

6 RESULTS AND DISCUSSION

In the following sections of this chapter, the main results are summarized and discussed in order to answer the research questions.
The Figure 31 illustrates the connections between the research question, published papers and the thesis key points. The surface control loop is visualizing the importance of linking the functional surface characterization to the function and manufacturing. The better understanding of surface topography is achieved by applying results suitable for application analysis in different areas: perception of gloss (paper1); medical application (paper2); tribological properties (paper3). Nevertheless all analysis includes some uncertainty accordingly to e.g: the method applied, measurement equipment used, environment influence, human influence, object characteristics. In this thesis uncertainty from the measurement instruments was a focus (paper3). In particular the metrological characteristics that influenced the measurements performed by CSI were studied and reported in paper4.

Paper 1, 2 and 3 cover two of the research questions formulated in the thesis. Different types of analysis techniques e.g: PSD, sets of surface roughness parameters, and motif analysis have been used in order to compare the measurement results of surface topography performed by different optical and tactile techniques. Paper 3 and the more extended paper 4 show the factors that influence the uncertainty of interferometric measurements, as well as pointing out calibration procedures needed to help determining and stating the metrological characteristics of the CSI.

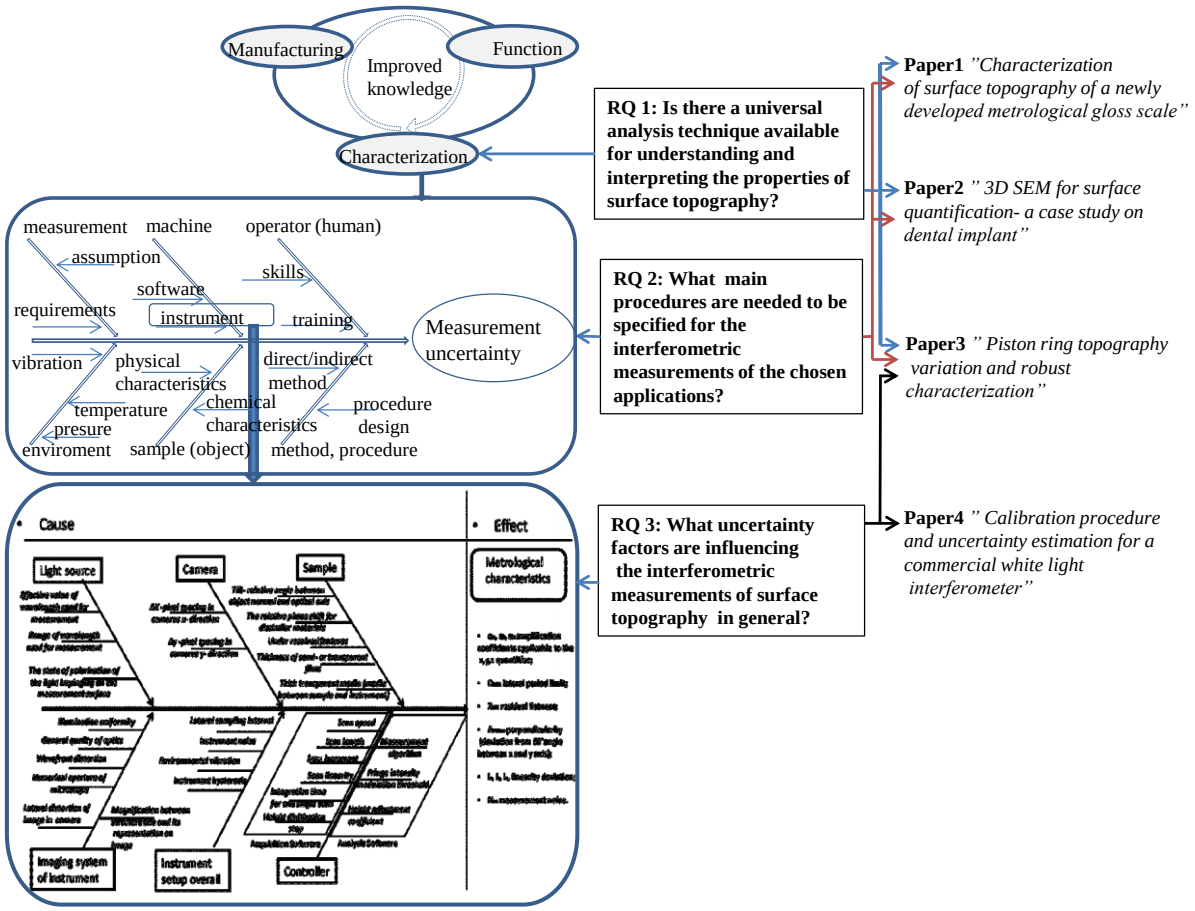

Figure 31: *Links between the research questions, published papers and the thesis structure.*

6.1 POWER SPECTRAL DENSITY (PSD) (PAPER1 Characterization of surface topography of a newly developed metrological gloss scale)

The study described in this paper shows how analysis and measurement techniques have been chosen for a certain application, which in turn contributes together with paper 2 and 3 to answering the research questions 1: ”Is there a universal analysis technique available for understanding and interpreting the properties of surface topography?” formulated in the thesis. The PSD has been used as an analysis technique for characterisation of surface topography of samples with different characteristics to find a correlation with the glossiness. The six samples with different refractive indices, different gloss levels and different roughness types have been examined in order to find characterization techniques for surface topography structures that may contribute to the perceived surface glossiness.

The instruments (CSI, Confocal Microscope CM, and AFM) and analysis techniques (PSD and Motif analysis) were chosen in order to be able to describe the surface structures in different spatial frequencies.

The PSD technique has been used for two purposes:

- For the comparison of measurement results achieved by using different instruments and
- For the comparison of different topographies on different samples.

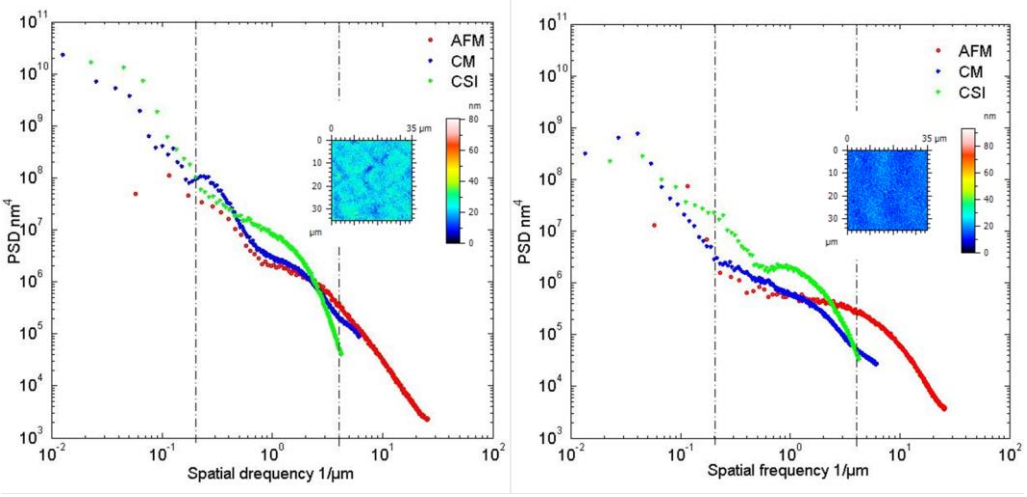

Figure 32: *Example of PSD analysis applied to the samples with same roughness and glossiness level but different refractive indices when measurements have been performed by different instruments (AFM, CM, CSI).*

Figure 32 demonstrates how PSD analysis was used for identification of the differences and equalities between instruments measuring similar topographies. The measurement instruments and techniques had different surface spatial wavelength band limits, so the measured roughnesses were not directly comparable. The PSD functions were calculated from the measurement data, and it rms roughnesses were obtained by integrating areas under the PSD curves between fixed upper and lower band limits. In this way, roughnesses measured with different instruments and techniques could be directly compared.

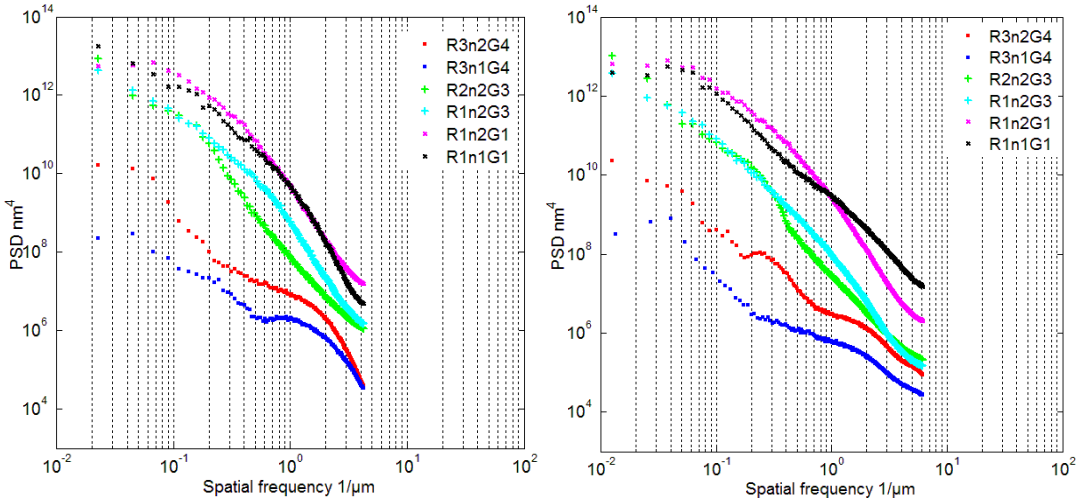

Figure 33: *PSDs for all samples, measurements by CSI (left) and CM (right).*

Figure 33 and table 6 shows how PSD has been used for the comparison of different topographies on different samples.

Usually all topographic images of the surfaces are based on data of surface heights, and need some modification for further analysis. The research question 2 formulates the importance of the procedure needed to be specified for the measurements of a chosen application. In the study described in the paper the data from CSI and CM measurements used for PSD calculations were aligned by subtracting a fitted least square plane from the raw heights for each data set. The presence of a curvature was observed in the AFM measurements, which can be explained by the action of the piezoelectric scanner that moves the probe. For this reason, measurements made by the AFM have been corrected by subtraction of a fitted line-by-line polynomial of 3rd degree order although it can be noted that this only has a minor influence on the result compared to using a plane for alignment.

Table 6: *Surfaces parameters with corresponding standard deviation calculated from measurements using different instruments.*

Instrument	AFM		CSI		CM	
Sample	$R_3n_2G_4$	$R_3n_1G_4$	$R_1n_1G_1$	$R_1n_2G_1$	$R_2n_2G_3$	$R_1n_2G_3$
Height Parameters						
S_q (nm)	5±0,2	4±0,4	100±8	102±6	277±25	201±42
S_z (nm)	96±16	31±1	466±76	1070±186	1663±174	1346±334

In addition to the analysis based on PSD, motif analysis has been applied to the measurements of all samples in different spatial frequency intervals. The aim was to give additional information regarding possibly important nano- and micro-features of the samples. Parameters such as peak area, and total number of peaks were examined. However no clear linear correlation was established between the feature parameters and the gloss of the samples, implying the strength of PSD analysis for connecting functional gloss to the optical analysis equipment. This part of the study addressed to point out the importance of suitable analysis techniques for a specific application and contributes to answering the RQ1.

6.2 SURFACE ROUGHNESS PARAMETERS (PAPER 2 - 3D SEM for surface quantification- a case study on dental implant)

In order to answer RQ1 this study uses the surface parameters as analysis techniques as well as characterization of surface properties based on measurements performed by optical techniques with different measurement principles. In this paper the comparison between measurements performed by CSI and a Scanning Electron Microscope SEM using 3D reconstruction techniques on the dental implant has been investigated in order to find an appropriate set of parameters for characterization of dental implant surfaces. Parameters from all families of surface roughness parameters have been included in thr study and relocation and resampling techniques were applied. Relocation and resampling are steps in procedure needed for the reliable comparison of instrument measurements and contribute to answer RQ2: "What main procedures are needed to be specified for the interferometric measurements of the chosen applications?"

It was found that for measurements using the same sampling distance SEM and Interferometer measurements normally for a majority of characterization parameters do not exceed 20% difference.

The SEM average amplitude parameters Sa, Sq are around 20% smaller than CSI ones. (see Figure 35). Several parameters, Smr, Sdr, Sdq, Spd, Spc are highly sampling dependent and can vary 56%- 100% between the high resolution- and re-sampled SEM measurements. The most differences between

SEM and Interferometer measurements for both high- and low resolution measurements were shown by the dale and hill parameters. Those parameters are heavily sampling dependent and for the dental implant huge variations (up to 900%) are found indicating the sensitivity of this set of 3D characterization parameters.

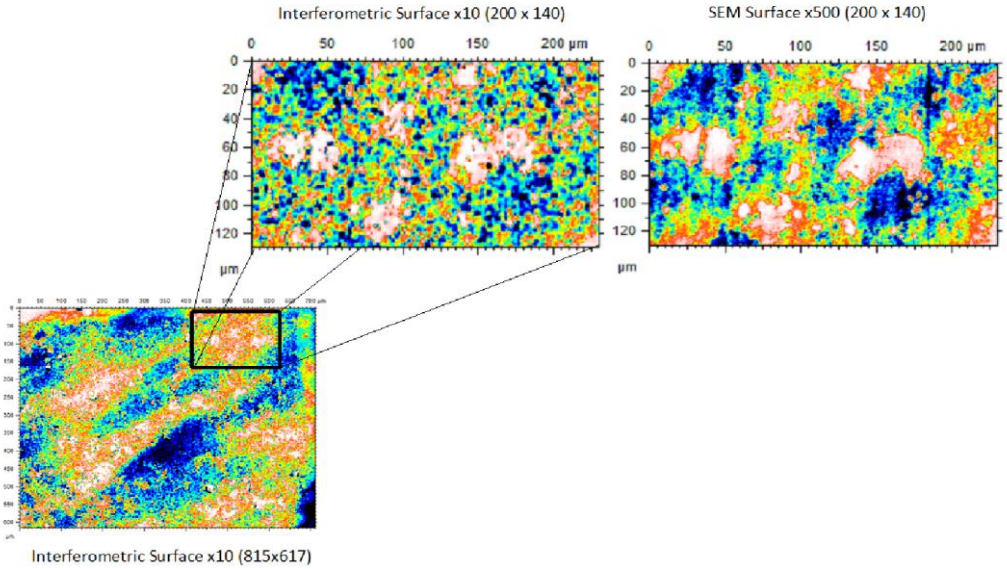

Figure 34: *Example of comparison using relocated areas for CSI and SEM.*

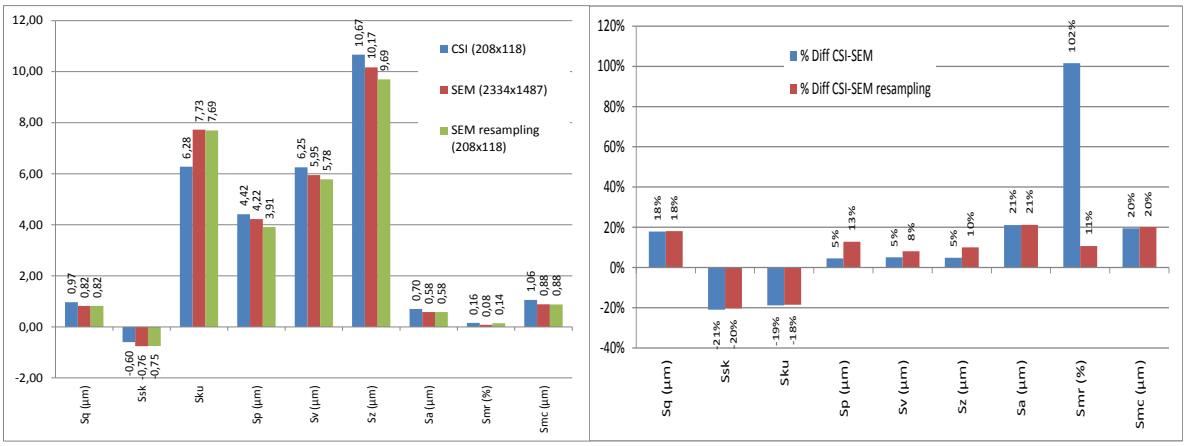

Figure 35: *Absolute value of differences of the parameters obtained using the SEM, the SEM re-sampling and the interferometer.*

The aim of comparison was by finding appropriate characterization techniques to show the usefulness of SEM with 3D reconstruction software for investigation of dental implant surfaces in different spatial frequency bands that contribute to satisfy RQ1. Related to RQ2 resampling and relocation techniques have been applied in the study to achieve comparable results from optical instruments based on different measurement principles.

6.3 SURFACE CHARACTERISATION AND UNCERTAINTY INFLUENCE ON RESULTS (PAPER 3 Piston ring topography variation and robust characterization)

This study was focused on the application to the investigation of a piston ring surface of an instrument built in-house, and the procedure for interferometric measurements as formulated in RQ2 has been of interest. Another aim of the study has been linked to RQ3: "What uncertainty factors are influencing the interferometric measurements of surface topography in general?". As the instrument is built in-house, validation of measurement can be assured by determination of measurement uncertainty.

In this paper a White Light Interferometer designed at Halmstad University has been used for non-destructive measurements of piston rings. For the validation of the measurement results achieved by the designed instrument a commercial interferometer has been used. The result of validation the instrument concludes that the instrument can be used for investigation of other types of surfaces, impossible to measure by a commercial interferometer (MicroXam). The instrument shows good repeatability of the height and functional parameters, but further investigation of instrument behavior in lower and higher measurement range is needed.

Another aim of study was to select the set of parameters from different families for characterization and production control of surface topography of twin oil piston rings. Experimental results have been provided to demonstrate the effectiveness of chosen parameters.

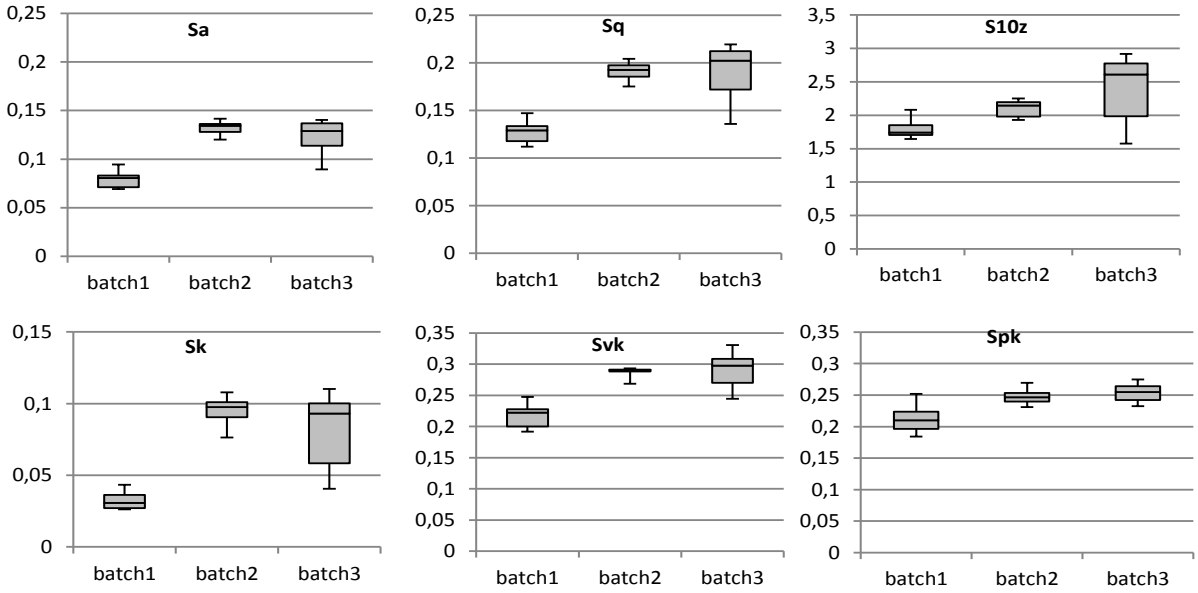

Figure 36: *Variations of the height and functional parameters according to each batch.*

From the measurements done with the WLI build at Halmstad University, the set of robust parameters for characterization of piston ring surfaces including Sa, Sq, Sk Spk, Svk, Str,Std have been selected. The Figure 36 shows that variation of chosen parameters both within batch and between rings was unexpectedly high. Those results give an answer to RQ1:" Is the universal analysis techniques available for understanding and interpreting the properties of surface topography?" The measurement uncertainties of parameters in z-scale were estimated to ±30nm, where instrument noise, repeatability and reproducibility were taken into account and in turn provide on RQ3. The best practice procedure for interferometric measurements in this application would be to use no filtering following a simple form removal for examination of piston ring surfaces, which contributes to answering RQ2.

6.4 CALIBRATION OF COMMERCIAL INSTRUMENT (PAPER 4 Calibration procedure and uncertainty estimation for a commercial white light interferometer)

The third research question focused on uncertainty factors that influenced the interferometric measurements and results from this study provide information on which metrological characteristics need to be investigated in order to perform reliable measurements.

So far no accepted standardized solutions exist for determination of measurement uncertainty for coherence scanning interferometers. An important issue that must be addressed to bring surface topography into compliance with manufacturing quality systems is the measurement traceability of the instruments.

This study explains the methods to quantify the influence of a number of metrological characteristics and uses metrologically accepted methods to calculate the corresponding measurement uncertainty.

The methodology includes simple steps to define the main metrological characteristics that influence the measurement uncertainty such as:

-measurement noise;
-flatness deviation;
-linearity errors;
-amplification coefficient;
-perpendicularity of axes;
-resolution of the measurements along the axis of operation.

The measurement noise and residual flatness deviation test showed that uncertainty contributions of those metrological characteristics were less than 1nm for both 10x and 50x magnification objectives. In addition information about the vertical resolution of the instrument can be retrieved from the measurement noise value, and was in our case determined to be 0,6nm for the WLI with 10x and 0,4nm for 50x magnifications objectives as seen from the results in table 7.
The calibration of the z-scale of the WLI has been performed on a groove depth standard with six grooves in the range from 0.282 to 9,44 µm. Figure 37 shows that the linearity errors' contribution to the uncertainty is significantly higher than the noise and flatness contributions

Table 7: *Measurement noise and residual flatness contribution to the uncertainty associated with measurements along z axis.*

Uncertainty contribution	**10x**	**50x**
$S_{q\ noise}$ (nm)	0,6	0,4
S_z (nm)	2,4	2,0
U_{NF} (nm)	0,9	0,7

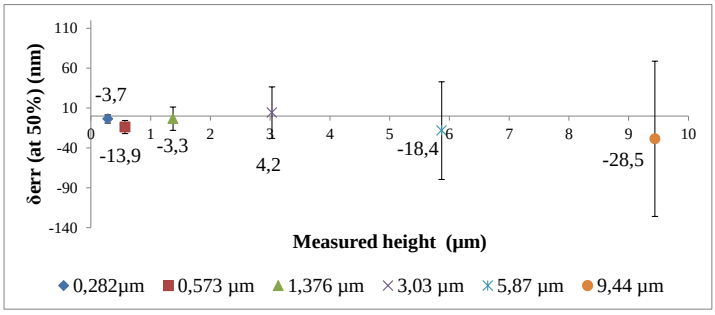

Figure 37: Plot of measurement error approximated of calibration of α_z and l_z of an instrument with 10x magnification objective.

Results in Table 8 shows that the uncertainty contribution from linearity errors, repeatability, reproducibility and traceability for the step-height up to 10µm is determined to be maximum 3% of the measured height for the 10x magnifications objective. For the 50x magnifications objective the maximum tested height was 2,8µm and the uncertainty contribution was determined to be maximum 4% of the measured height.

Table 8: *Amplification and linearity contribution to the z measurement uncertainty.*

Nominal height (µm)	$U_{T\text{-}z}$ **(nm)**	
	10x	**50x**
0,282	5,8	12,4
0,571	15,7	9,9
1,374	14,8	
2,80		78,0
3,03	32,0	
5,87	63,6	
9,44	100,9	

The calibration procedure of the x and y scale of the instrument showed the linear trend in residual errors determination demonstrated by Figure 38.

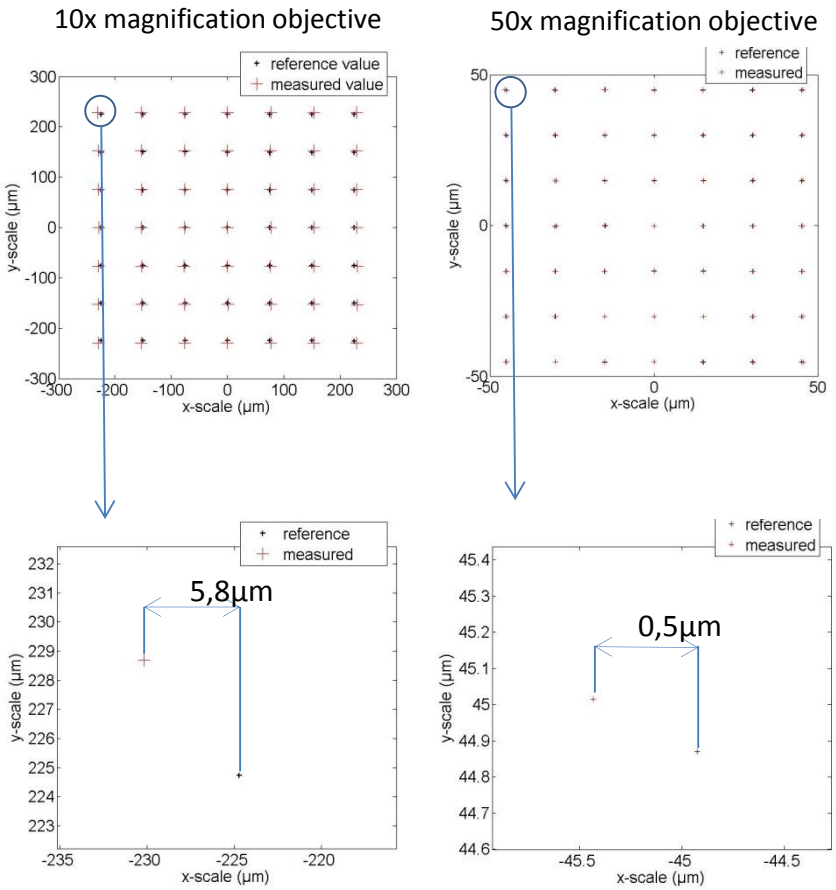

Figure 38: *Plot of measurement error approximated of calibration of a WLI equipped with 10x magnifications -left and 50x-magnifications objective-right.*

This effect can be partly corrected by applying a common amplification coefficient for x and y scales. In this study no adjustment has been performed and the contribution to uncertainty has been calculated using unadjusted linearity error values.

The lateral resolution contributing to the measurement uncertainty plays the dominant role in the combined measurement uncertainty for the x and y-scale, and based on lateral period limit determination. The lateral period limit estimated from the measurements performed by WLI with 50x magnification objective was 1,7µm with standard deviation 0,08µm. The standard measurement uncertainty associated with the calibration of the lateral period limit of the WLI used here is

U_{Res}=1 µm. Some consideration should be made in the case of lateral period limit determination, as the achieved value is influenced by quality of the artefact, pixel size of the instrument, measurements conditions (noise, vibration).

The calibration procedure that includes measurements on artefacts listed in study provides guidance to estimate the uncertainty of measurements performed by CSI, that was of interest in RQ3.

7 CONCLUSIONS AND FUTURE WORK

This chapter summarizes the main conclusions and suggests future research work.

7.1 CONCLUSIONS

The aim of this thesis was to increase the current knowledge of the interaction between surfaces and the optical metrology of surfaces' topographical properties.

Within the current research scope the following conclusions can be drawn (the numbers below refer to the numbered questions formulated in section 1.3).

RQ1: *Is there a universal analysis technique available for understanding and interpreting the properties of surface topography?*

(1) There are numerous analysis techniques for surface topography characterization. Independent of analysis technique, the most accepted and used measures to characterize surface topography by industry and scientists are surface roughness parameters. Frequently, for a better understanding and interpretation of the properties of a surface, a combination of different techniques can be necessary. Another important role of different analysis techniques are to compare of measurement results achieved by different instruments: e.g. tactile and optical instruments. The use of PSD analysis in this thesis showed it to be an analysis tool for identification of the differences and equalities between instruments measuring similar topographies, enabling a selection of the proper instruments for measuring topographies at given spatial frequencies or combination of frequencies.

RQ2: *What main procedures are needed to be specified for the interferometric measurements of the chosen applications?*

(2) According to different applications, the methodology for each case needs to be listed. It is important that new instruments are tested for some specific applications and that the influences of the main metrological characteristics on measurement results are considered.

RQ3: *What uncertainty factors are influencing the interferometric measurements of surface topography in general?*

(3) The determination of measurement uncertainty is important when evaluating a measurement result and judging its significance. For the determination of uncertainty, a calibration procedure, that covers all significant contributions to the measurement uncertainty budget for the specific measurement instrument, is needed. The main metrological characteristics for CSI and their influence on the measurement uncertainty were investigated. The dominant component for uncertainty estimation in the z-scale for CSI is the noise contribution and the dominant component for the x- and y- scale is the lateral resolution.

7.2 FUTURE WORK

Suggestions for future work based on the results in this thesis are as follows:

- Empirical and analytical study of spatial content of surfaces for different applications. For this purpose comparison of different instruments and different analysis should be combined to create the methodology for understanding of surface properties.

- Further investigation of metrological characteristics influencing the measurement uncertainty of CSI would be useful by developing parts of the calibration procedure of

CSI e.g influence of light source spectra on determination of the modulation envelope, self-calibration procedure for lateral correction of CSI x,y-axes.

- Develop a good practice guide to assist users in achieving a valid surface measurement on surfaces exhibiting roughness, texture and structures, using the technique of coherence scanning interferometry (CSI).

REFERENCES

[1] R. Leach, C. Evans, L. He, A. Davies, A. Duparré, A. Henning, C.W Jones, D. O'Connor, *"Open questions in surface topography measurement: a roadmap"*, Surf. Topogr.: Metrol. Prop. 3, 2015.

[2] ISO 25178-2 2012 Geometrical product specifications (GPS)— Surface texture: Areal - Part 2: Terms, definitions and surface texture parameters (Geneva: International Organization for Standardization).

[3] J.-A. Beraldin, D. Mackinnon, L. Cournoyer, *"Metrological characterization of 3D imaging systems: progress report on standards developments"*, 17th International Congress of Metrology, 13003, 2015.

[4] R.K. Leach, *"Some issues of traceability in the field of surface topography measurement"*, Wear, 257/12, 1246-1249, 2004.

[5] K.J.Stout, J.Davis, *"Surface topography of cylinder bores-the relationship between manufacture, characterization and function"*, Wear 95(2), p.111-125, 1984.

[6] http://kcdb.bipm.org/default.asp.

[7] JCGM 200:2008. *International Vocabulary of Metrology – Basic and general concepts and associated terms*, 3rd Edition. Joint Committee for Guides in Metrology.

[8] BIMP, IEC, IFCC, ISO, IUPAC, IUPAP, OIML, *Guide to the Expression of Uncertainty in Measurement*, ISO, Geneva, 1993.

[9] JCGM 100:2008. *Evaluation of measurement data – Guide to the expression of uncertainty in measurement*, Joint Committee for Guides in Metrology.

[10] ISO/IEC 98-3, Uncertainty of Measurement – Part 3: *Guide to the Expression of Uncertainty in Measurement*, ISO Edition, Geneva, Switzerland, 2010.

[11] V.R.Meyer, *"Measurement uncertainty",* Journal of Chromatography A, 1158, 15–24, 2007

[12] W. Kessel, *"Measurement uncertainty according to ISO/BIMP-GUM",* Thermocimica Acta 382, 1-16, 2002.

[13] M.Wolf, *"A Modeling Language for Measurement Uncertainty Evaluation"*, PhD Thesis, 2009.

[14] ISO 14253-2:2011 Geometrical product specifications (GPS) -- Inspection by measurement of workpieces and measuring equipment -- Part 2: Guidance for the estimation of uncertainty in GPS measurement, in calibration of measuring equipment and in product verification parameters (Geneva: International Organization for Standardization).

[15] K.Birch*, "Estimating Uncertainties in Testing"* Measurement Good Practice Guide No. 36.

[16] F. E. Satterthwaite. *"An approximate distribution of estimates of variance components",* Biometrics Bulletin, 2(6):110–114, 1946.

[17] Supplement 1 of ISO GUM 95, JCGM 101:2008 – Evaluation of Measurement Data – Supplement 1 to the Guide to the Expression of Uncertainty in Measurement – Propagation of Distributions Using a Monte Carlo Method BIPM, IEC, IFCC, ILAC, ISO, IUPAC, IUPAP and OIML, first ed., Sevres, France, 2008.

[18] P.R.G. Couto, J.C. Damasceno, S.P. de Oliveira, *Monte Carlo simulations applied to uncertainty in measurement*, Theory and Applications of Monte Carlo Simulations, InTech Publisher, 2013, pp. 27–51, http://dx.doi.org/10.5772/53014 (Chapter 2).

[19] M.A. Herrador, A.G. González, *Evaluation of measurement uncertainty in analytical assays by means of Monte-Carlo simulation*, Talanta 64, 415–422, 2004.

[20] ISO 25178-6: 2010 Geometrical product specifications (GPS)—*Surface texture: areal—Part 6: Classification of methods for measuring surface texture*, (Geneva: International Organization for Standardization)

[21] J. M. Bennett, J. H. Dancy, *"Stylus profiling instrument for measuring statistical properties of smooth optical surfaces",* Appl. Opt. 20, 1785–1802, 1981.
[22] J. M. Bennett, L. Mattson, *"Introduction to surface roughness and scattering",* Optical Society of America, Washington, D.C., 1989.
[23] J. M.Bennett, V. Elings, K. Kjoller, *"Precision metrology for studying optical surfaces",* Opt. Photonics News, 2, 14–18, 1991.
[24] G. A. Al-Jumaily, S. R. Wilson, K. C. Jungling, J. R. Mcneil, J. M. Bennett, *"Frequency response characteristics of a mechanical stylus profilometer",* Opt. Eng., 26, 953–958, 1987.
[25] D-H. Lee, and N-G. Cho, *"Assessment of surface profile data acquired by a stylus profilometer",* Measurement Science and Technology, Volume 23, Number 10, 2012.
[26] V.L.Mironov, *"Fundamentals of scanning probe microscopy",* The Russian academy of sciences institute for physics of microstructures, Nizhniy Novgorod, 2004.
[27] S. Alexander, L. Hellemans, O. M. J. Schneir, V. Elings, P. K. Hansma, M. Longmire, J. Gurley, *"An atomic-resolution atomic-force microscope implemented using an optical lever",* Applied Phys., 65, 164–167, 1989.
[28] D. Sarid , D. Iams, V. Weissenberger, L. S. Bell, *"Compact scanning force microscope using a laser diode",* Opt. Lett., 13, 1057–1059, 1988.
[29] R.W. Carpick, D.F. Ogletree, M. Salmeron, "*Lateral stiffness: A new nanomechanical measurement for the determination of shear strengths with friction force microscopy",* Appl. Phys. Lett. 70, 1548–1550, 1997.
[30] C.T. Gibson, G.S. Watson, S. Myhra, "*Lateral force microscopy – a quantitative approach",* Wear 213, 72–79, 1997.
[31] I. Schmitz, M. Schreiner, G. Friedbacher, M. Grasserbauer, "*Phase imaging as an extension to tapping mode AFM for the identification of material properties on humidity-sensitive surfaces",* Appl. Surf. Sci. 115, 190–198, 1997.
[32] R.S. McLean, B.B. Sauer, *Tapping-mode AFM studies using phase detection for resolution of nanophases in segmented polyurethanes and other block copolymers,* Macromolecules 30, 8314–8317, 1997.
[33] R. Garcia, R. Perez, "*Dynamic atomic force microscopy methods",* Surf. Sci. Rep. 47, 197–301, 2002.
[34] F.J. Giessibl, *"Atomic resolution of the silicon (111)-(7x7) Surface by atomic force microscopy",* Science 267, 68–71, 1995.
[35] M. Minsky, *Microscopy Apparatus*, US Patent No. 3,013,467, 1961.
[36] D. Malacara, *Optical shop testing*.NewYork:Wiley; pp.689-695, 2007.
[37] A.K. Ruprecht, T.F.Wiesendanger, H.J.Tiziani, *"Chromatic confocal microscopy with a finite pinhole size",* Opt.Lett., 29,2130-2132, 2004.
[38] H.J.Tiziani, H.M. Uhde, *"Three dimensional image sensing by chromatic confocal microscopy",* Appl Opt., 33, 1838-1843, 1994.
[39] H.J.Tiziani, M.Wagner, D.Steudle, *"Confocal principle for macro- and microscopic surface and defect analysis",* Opt. Eng., 39, 32-39, 2000.
[40] D.Malacara, M.Servı´n, Z. Malacara, *"Interferogram analysis for optical testing",* New York: Marcel Dekker; 247–248, 1998 .
[41] J.Schwider, *"Advanced evaluation techniques in interferometry",* in: Progress in Optics, Vol. XXVIII, E.Wolf, editor. Elsevier Science; 274–276,1990.
[42] E.P.Goodman, J.C.Wyant, *"Field guide to interferometric optical testing",* Washington: SPIE Press; 32–36,2006.
[43] J.Schreiber, Horst, J. H. Bruning. *"Phase shifting interferometry."* Optical Shop Testing, Third Edition, 547-666, 2006.
[44] K.Creath , *"Step height measurement using two-wavelength phase-shifting interferometry",* Appl. Opt., 26, 2810, 1987a.